Georgia Institute of Technology

Phenomena Identification and Ranking Tables (PIRTs) Report for Material Selection and Possible Material Degradation Mechanisms in FHR

School of Materials Science and Engineering
Georgia Institute of Technology
Atlanta, GA 30332

Issue Date: April 15, 2017

Phenomena Identification and Ranking Tables (PIRTs) Report for Material Selection and Possible Material Degradation Mechanisms in FHR

Panel Members:

David Diamond (BNL, Facilitator)
Farzad Rahnema (Georgia Tech)
Preet M. Singh (Georgia Tech)
Grayon Yoder (ORNL)
Weiju Ren (ORNL)
Jinsuo Zhang (Ohio State Univ., Virginia Tech)
Jim Keiser (ORNL)
Dane Wilson (Thorcon Power)
Sam Sham (ANL)
William Corwin (DOE, Nuclear Energy)
Vinay Deodeshmukh (Haynes International)
Chaitanya Deo (Georgia Tech)
Kevin Chan (Georgia Tech)

Prepared by:

Preet M. Singh, Kevin Chan, and Farzad Rahnema
Georgia Institute of Technology,
Atlanta, Georgia

Acknowledgement

This work is being performed using funding received from the U.S. Department of Energy Office of Nuclear Energy's Nuclear Energy University Programs.

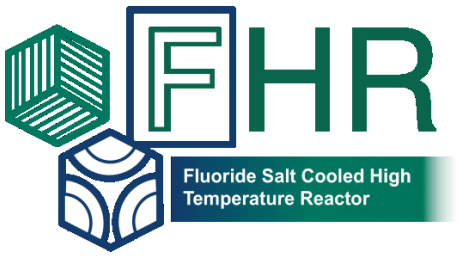

Executive Summary

Material selection and identification of the possible degradation mechanisms for the selected materials in FHRs is important for the licensure and the safe operation of Fluoride High-Temperature Reactors (FHRs). In order to address this task, the GT led IRP hosted a Phenomena Identification and Ranking Table (PIRT) panel of internal and invited external experts to address degradation mechanisms and other materials related issues of importance to the FHRs. The PIRT panel for the FHR-IRP on Materials met on November 28-30, 2016 at Georgia Tech. The panel was led by Dr. David Diamond, and consisted of both internal and external experts on different materials and related degradation mechanisms of interest for the FHR technologies. Student observers with an interest in materials related activities also attended this PIRT exercise.

Materials, ones that come in contact with FLiBe or FLiNaK molten salts or other related environments like high temperature steam etc., were considered in this PIRT. There is limited experience with molten salts, so identifying and ranking of the possible degradation mechanisms in these environments was the primary objective of this PIRT. Secondary objective was to rank the degradation mechanisms in more known environments, like in high temperature steam. Focus of this PIRT was the metallic alloys used in FHRs, and it was acknowledged that non-metallic materials like graphite, pyrolytic carbon, and ceramics require a separate PIRT exercise. Degradation mechanisms considered in this PIRT included chemical degradation, mechanical degradation, radiation degradation, and synergistic effect of these mechanisms that may negatively impact operations or cause some safety concerns for the major structural components of FHRs. Specific mechanisms of degradation for each class were defined and considered individually. Although degradation mechanisms will depend on the materials used and the mechanical, chemical or radiation conditions, for this PIRT exercise the ORNL pre-conceptual design for the Advance High Temperature Reactor (AHTR) was selected as the candidate design. Environments considered for the degradation phenomenon were based on this reactor design parameters. Where the environmental parameters for a component were not available, important degradation mechanisms under extreme conditions were considered. Main components which were considered included vessel and primary piping, primary heat exchangers, steam generator vessel, steam generator tubes, intermediate loop piping, valves and pumps. Welds in all structural components were identified as an important class of material, which varies in composition and properties, and needs more attention. Importance of impurity control in molten fluorides considered for FHR was highlighted throughout PIRT panel discussions.

All identified degradation mechanisms (phenomena) for the materials were evaluated and ranked for their potential impact on the safe functioning of specific FHR component as well as on the basis of knowledge level for a given phenomenon under operating conditions considered for that component. PIRT process is described in detail and the phenomenon ranking tables based on panel discussions are included in this report.

Table of Contents

List of Figures

List of Tables

List of Abbreviations

AGR	Advanced Gas Reactor
AHTR	Advanced High Temperature Reactor
C-C	Carbon-Carbon

CF	Corrosion Fatigue
CHM	Carbon to Heavy Metal
DOE	U.S. Department of Energy
DRACS	Direct Reactor Auxiliary Cooling System
FOM	Figure of Merit
FHR	Fluoride High Temperature Reactor
GT	Georgia Institute of Technology
HTGR	High Temperature Gas Reactor
IRP	Integrated Research Project
NEUP	Nuclear Energy University Programs
OD	Outer Diameter
ORNL	Oak Ridge National Laboratory
OSU	The Ohio State University
PBR	Pebble Bed Reactor
PIRT	Phenomena Identification and Ranking Table
RPT	Reactivity-Equivalent Physical Transformation
RSICC	Radiation Safety Information Computational Center
SCC	Stress Corrosion Cracking
SINAP	Shanghai Institute of Applied Physics
SS	Stainless Steel
TAMU	Texas A&M University
TAMU-K	Texas A&M University, Kingston
TRISO	Tristructural-Isotropic
VHTR	Very High Temperature Reactor
V&V	Verification and Validation

1. Introduction

1.1. Background

The widespread deployment of Fluoride High-Temperature Reactor (FHR) technology promises many benefits: improved safety through passive safety systems and proliferation-resistant waste forms; improved economics through higher operating temperatures and thus higher operating efficiency; and a diversification of the nation's energy portfolio by expanding the role of nuclear power beyond baseload electricity to meeting peaking electricity demand and supplying industrial process heat. Several challenges remain before this class of reactors can be deployed, mostly related to its technological readiness. Realizing this need, the U.S. Department of Energy (DOE) initiated an Integrated Research Project (IRP) to address the technology gaps for FHR deployment.

1.2. PIRT Panelists

Experts from different fields of materials science and engineering, mechanical behavior of materials, nuclear materials, and environmental degradation of materials participated in the PIRT. This PIRT exercise was dedicated to identifying and ranking of the possible degradation mechanisms for metallic materials in FHR environments that may come in contact with FLiBe or FLiNaK molten salts or other FHR related environments like high temperature steam etc,. PIRT panel had 10 voting members. Georgia Tech students, Kevin Chen (graduate), and Rebecca Ambrecht (undergraduate) were observers and scribe for this meeting. Dr. David Diamond led the PIRT Panel and acted as the facilitator for the process.

Table 1-1: FHR Material PIRT panelists and organization.

Name	Organization
David Diamond (Facilitator)	***Brookhaven National Laboratory***
Preet M. Singh	***Georgia Institute of Technology***
Grayon Yoder	***Oak Ridge National Laboratory***
Weiju Ren	***Oak Ridge National Laboratory***
Jinsuo Zhang	***Ohio State University (now at Virginia Tech)***
Jim Keiser	***Oak Ridge National Laboratory***
Dane Wilson	***ThorCon Power***
Sam Sham	***Argonne National Laboratory***
***William Corwin**	***Department of Energy, Nuclear Energy***
Vinay Deodeshmukh	***Haynes International***
Chaitanya Deo	***Georgia Institute of Technology***
Farzad Rahnema	***Georgia Institute of Technology***

** Attended via teleconference facility*

1.3. PIRT Overview

As a starting point for the panelists, a whitepaper on *Material Selection and Possible Material Degradation Mechanisms in FHR* was compiled and provided before the meeting to perform the following roles in preparation for the meeting:

- Present the AHTR Design Concept and Materials considered for the main components
- Brief summary of previous Materials related work for the AHTR
- Identify possible material degradation mechanisms related to FHR environments
- Identify variables that are important for of material behavior/degradation mechanisms in FHRs

The AHTR design concept considered as the basis for the PIRT exercise was a Fluoride High-Temperature Reactor (FHR) with a primary coolant of FLiBe ($2LiF\text{-}BeF_2$), as described in section 3 of this report. The most recent revision of the FHR pre-conceptual design was provided, as a part of the whitepaper to the PIRT panel, with an emphasis on reactor components and the materials for different chemical and physical environments in FHR. A short summary of materials selected for FHR and their performance in molten salt coolants and other FHR related environments was prepared. Although different classes of materials (i.e. metallic alloys, carbonaceous materials like graphite, pyrolytic carbon, and ceramics like SiC and BC) will be used for different components of FHR and were discussed in this PIRT like exercise, the main emphasis during the PIRT meeting was on the metallic materials and their degradation mechanisms. A list of possible degradation mechanisms, including chemical degradation, mechanical degradation, thermal degradation, and radiation damage was listed and the effect of different environmental variables was summarized in this report. This list does not represent every degradation mechanism or degradation phenomenon possible and does not discuss all synergistic effects of damage mechanisms on material behavior. This list may also include some items which are deemed to have minimal impact on material degradation of selected classes of materials in FHR related environments.

The PIRT process consisted of following steps:

Step 1: Define the Issue
Materials used in the FHR, ones that come in contact with FLiBe or FLiNaK molten salts or other related environments like high temperature steam etc., need to be capable of providing functionality with high reliability, to provide safe and economical operation. There is limited experience with molten salts, so identifying and ranking of the possible degradation mechanisms in these environments was the primary objective of this PIRT. Secondary objective was to rank the degradation mechanisms in more known environments, like in high temperature steam. Degradation mechanisms considered in this PIRT included Chemical Degradation, Mechanical Degradation, Radiation Degradation, and synergistic effect of these mechanisms, that may negatively impact operations or cause some safety concerns for the major structural components of FHRs.

Step 2: Define objectives of the PIRT
Determine the materials and their associated degradation mechanisms that might negatively impact operation of the FHR and determine new experimental databases, modeling, and detailed analysis needs to be carried out.

- Definition of "Operation" for this PIRT includes transients and accidents
- Initial focus on structural materials
- Secondary focus on core, control rod, instrumentation materials

Step 3: Define Hardware, Scenario, Methodology
AHTR with materials (structural, core, etc.) given in White Paper by Georgia Tech (GT) and expanded upon by panel. White Paper and presentations given by various experts on different aspects of AHTR design, materials, and mechanical behavior were used to define the environmental parameters for this PIRT process. The environmental parameters, including salt chemistry, salt impurities, temperature, stress state, irradiation fluence and flux etc. for this PIRT process were defined based on: (a) Georgia Tech (GT) White Paper on AHTR materials (structural, core, etc.). Review of this AHTR conceptual design is also presented in section 3 of this report; (b) presentations by various panel experts on different aspects of AHTR design, materials, and mechanical behavior; and (c) consensus opinions of the panel. Each table defines the environment considered for that particular component considered in this PIRT. Normal operation as well as transients/accident conditions for most of critical components of FHR were considered.

STEP 4: Define Evaluation Criteria, Figures-of-Merit (FOM)
Figure of merit for different components is different, depending on the risks involved with the failure of that component and its expected service life. Various criteria for unacceptable degradation, used as FOM for the PIRT process included the following:

- Any crack (e.g stress corrosion, corrosion fatigue, fatigue cracking)
- "Excessive" embrittlement (radiation induced, hydrogen embrittlement and other embrittlement sources)
- Decrease in fracture toughness, increase in yield strength
- "Excessive" deformation
- Loss of functionality
- others

Step 5: Identify, Obtain, Review Database
Important references related to the FHR material selection were sent to panel. Whitepaper for the PIRT also included the AHTR design information along with the degradation mechanisms.

Step 6: Identify Phenomena (processes, parameters, etc)

Phenomena discussed in this PIRT included a number of degradation mechanisms that can potentially cause enough damage to cause local failure in the components considered in this PIRT. Details of these mechanisms are given in a separate section after PIRT tables in this report. However, the phenomena could be grouped under following degradation categories:

- Degradation Mechanisms
    - Chemical Degradation
    - Mechanical Degradation
    - Radiation Degradation
    - Synergistic Effect

Possibility of any selected alloy or material to fail by the degradation mechanism will depend on the environmental factors as well as other influencing factors listed here.

- Add in Influencing Factors
    - Environment (including salt chemistry, salt impurities, temperature, stress state, irradiation fluence and flux etc.)
    - Fabrication method (e.g welding)
    - Geometry
    - Impurities in molten salt

Step 7: Rank Importance and *Rationale*

Importance of any degradation mechanism for a given component was ranked based on its influence on the figure of merit (FOM) for that particular component. Table below describes the lettered ranking used in the PIRT.

Table 1-2: Description of degradation mechanism FoM ranking designations.

Ranking	***Description***
High (H)	**Significant or dominant influence on FoM**
Medium (M)	**Moderate influence on FoM**
Low (L)	**Small influence on FoM (including the possibility that the phenomenon is not present or possible) ("Low" means knowledge level is not considered)**

Step 8: Assess Uncertainty (Knowledge Level)

Based on the data and the information available to the experts participating in the PIRT process, each phenomenon (degradation mechanism for a given material in a given environment) was ranked. Table below describes the lettered ranking of knowledge level for each phenomenon considered in this PIRT.

Table 1-3: Description of knowledge level ranking designations.

Ranking	***Description***
Known (K)	**Phenomenon is well understood, and can be accurately modeled/analyzed/assessed.**
Partially Known (P)	**Phenomenon is understood, however, can only be modeled with moderate uncertainty.**
Unknown (U)	**Phenomenon is not well understood. Modeling the phenomenon is currently either not possible or is possible only with large uncertainty.**

Determining Phenomena That Need Further Consideration

Based on the importance ranking and knowledge level for a given phenomenon (Degradation mechanism in a given environment for a given material), phenomenon that need further consideration can be selected by the following criteria shown in the table below as an example.

Table 1-4: Knowledge level and importance ranking combinations which need further consideration.

		Importance Ranking		
		H	**M**	**L**
Knowledge Level	**K**			
	P	**YES**		
	U	**YES**	**YES**	

Document Results and *Conclusions*

Discussion of each individual degradation mechanism and its possibility was considered for every selected material for every FHR component considered in this PIRT process. This provided the rationale for all rankings in the tables in the next section. Based on these discussions, data available, and the knowledge of experts on the PIRT panel, research needs and gap analysis was done to identify research needs for each specific phenomenon considered.

2. PIRT Tables

2.1. Vessel and Primary Piping

Table 2-1a: PIRT table for Vessel and Primary Piping made of Alloy 800-H with Ni cladding.

Component: Vessel and Primary Piping					
Environment: 700C steady state, up to 760C transient; 40-60 years; stress levels will vary; 10^20 n/cm^2					
Material: Alloy 800-H with Ni cladding			**Comment:**		
Phenomenon	**Importance Score (Final)**	**Comments**	**Knowledge Level**	**Comments**	**Path Forward**
Chemical Degradation Mechanisms					
Temperature-Gradient Driven Corrosion/deposition	L	Higher impurity levels will exacerbate this phenomenon. Thickness dependent (interdiffusion)			
Galvanic Corrosion	L				
Localized Selective Dissolution	L				
Intergranular Corrosion	L	Thickness and interdiffusion dependent.			
Flow Accelerated Corrosion	L				
High Temperature Oxidation	M	Outside surface	K	Important for the vessel and piping parts exposed to air at high temperature	
Hydrogen (Tritium) Related Degradation [Hydride formation - embrittlement]	L				
Impurity effect [Fission products, Tritium Fluoride (TF)]	L	Assuming redox control			
Fluorine attack under solidification conditions	L	No solidification expected			
Cladding Interdiffusion	H	Thickness dependent	P		Literature search for interdiffusion data and identify known interdiffusion models. Need validation experiments for different process conditions and temperatures.
Cladding Delamination	H	Dependent on fabrication process and QC	P		Literature search, and get information from Sandvik, Special Metals, WSI welding services, Sumitomo, and Klad. Also look at work from LANL, ORNL, UNLV, Univ. of Florida, and MIT. Review ASTM specification. Review in service examination methods [changes in microstructure over time or radiation effects]. Develop experimental techniques for this material.

Mechanical Degradation Mechanisms					
Thermal Aging	M		K	Alloy 800-H already in ASME code	
Creep	H		P	Known for 800-H, but unknown for Ni cladding	Perform long term creep-rupture tests to support the design lifetime. Investigate possible microstructure and property changes for the coupled materials.
Fatigue [LCF, Thermal fatigue] (800-H)	M		K	Known for 800-H, but unknown for Ni cladding	
Fatigue [LCF, Thermal fatigue] (Ni cladding)	H	Cracking of clad layer will expose shell to molten salt	U	Known for 800-H, but unknown for Ni cladding	Perform fatigue tests to develop S-N curves of both nickel and the coupled materials.
Creep-Fatigue	H	Cracking of clad layer will expose shell to molten salt	U	Known for 800-H, but unknown for Ni cladding	Perform tests to quantify creep-fatigue interaction of both nickel and coupled materials.
Erosion/Wear	L	Assuming velocities are low			
Crack Growth	H	High for Ni cladding, Moderate for Alloy 800-H	U	Maybe known for 800-H, but unknown for Ni cladding	Literature search. Perform tests to develop creep, fatigue, and creep-fatigue crack growth data. These tests may need to be done for both nickel and coupled materials.
Stress relaxation cracking (SRC)	H	Can be high for Alloy 800-H. Related to weldment and other fabrication processes.	K		
Radiation Degradation Mechanisms					
Irradiation Embrittlement	H	Assuming 10^20 n/cm^2	U	Unknown for Ni	Literature search. Do scoping computational simulations before tests. Perform irradiation tests of coupled material to investigate embrittlement phenomena. Determine embrittlement dose level threshold.
Irradiation Swelling	L	Assuming < 10^20 n/cm^2			
Irradiation Creep	L	Assuming < 10^20 n/cm^2			
Irradiation Assisted Stress Corrosion Cracking/Corrosion fatigue	M	Assuming < 10^20 n/cm^2	U		Literature search. Perform irradiation tests of coupled material to investigate irradiation assisted SCC/CF.

Table 2-1b: PIRT table for Vessel and Primary Piping made of Alloy 800-H with Alloy N cladding.

Component: Vessel and Primary Piping					
Environment: 700C steady state, up to 760C transient; 40-60 years; stress levels will vary; 10^20 n/cm^2					
Material: Alloy 800-H with Alloy N cladding			**Comment:**		
Phenomenon	**Importance Score (Final)**	**Comments**	**Knowledge Level**	**Comments**	**Path Forward**
Chemical Degradation Mechanisms					
Temperature-Gradient Driven Corrosion/deposition	H	Higher impurity levels will exacerbate this phenomenon.	K		
Galvanic Corrosion	L				
Localized Selective Dissolution	L				
Intergranular Corrosion	L	Thickness and interdiffusion dependent.			
Flow Accelerated Corrosion	L				
High Temperature Oxidation	M	Outside surface	K		
Hydrogen (Tritium) Related Degradation [Hydride formation - embrittlement]	L				
Impurity effect [Fission products, Tritium Fluoride (TF)]	L	Assuming redox control			
Fluorine attack under solidification conditions	L	No solidification expected			
Cladding Interdiffusion	H	Thickness dependent	P		Literature search for interdiffusion data and identify known interdiffusion models. Need validation experiments for different process conditions and temperatures.
Cladding Delamination	H	Dependent on fabrication process and QC	P		Literature search, and get information from Sandvik, Special Metals, WSI welding services, Sumitomo, and Klad. Also look at work from LANL, ORNL, UNLV, Univ. of Florida, and MIT. Review ASTM specification. Review in service examination methods [changes in microstructure over time or radiation effects]. Develop experimental techniques for this material.
Mechanical Degradation Mechanisms					
Thermal Aging	M		K	Alloy 800-H already in ASME code	
Creep	H	Cracking of clad layer will expose shell to molten salt	P	Known for 800-H, but unknown for Alloy N cladding	Perform long term creep-rupture tests to support the design lifetime. Investigate possible microstructure and property changes for the coupled materials.
Fatigue [LCF, Thermal fatigue] (800-H)	M		K		
Fatigue [LCF, Thermal fatigue] (Alloy N cladding)	H	Cracking of clad layer will expose shell to molten salt	U	Known for 800-H, but unknown	Perform fatigue tests to develop S-N curves of both Alloy N and the coupled materials.

				for Alloy N cladding	
Creep-Fatigue	H	Cracking of clad layer will expose shell to molten salt	U	Known for 800-H, but unknown for Alloy N cladding	Perform tests to quantify creep-fatigue interaction of both Alloy N and coupled materials.
Erosion/Wear	L	Assuming velocities are low			
Crack Growth	H	High for Alloy N cladding, Moderate for Alloy 800-H	U	Maybe known for 800-H, but unknown for Alloy N cladding	Literature search. Perform tests to develop creep, fatigue, and creep-fatigue crack growth data. These tests may need to be done for both Alloy N and coupled materials.
Stress relaxation cracking (SRC)	H	Can be high for Alloy 800-H. Related to weldment and other fabrication processes.	K		
Radiation Degradation Mechanisms					
Irradiation Embrittlement	H	Assuming 10^20 n/cm^2	K	Known from MSRE data	
Irradiation Swelling	L	Assuming < 10^20 n/cm^2			
Irradiation Creep	L	Assuming < 10^20 n/cm^2			
Irradiation Assisted Stress Corrosion Cracking/Corrosion fatigue	M	Assuming < 10^20 n/cm^2	U		Literature search. Do scoping computational simulations before tests. Perform irradiation tests of coupled material to investigate irradiation assisted SCC/CF.

Table 2-1c: PIRT table for Vessel and Primary Piping made of SS 316H with Ni cladding.

Component: Vessel and Primary Piping					
Environment: 700C steady state, up to 760C transient; 40-60 years; stress levels will vary; 10^20 n/cm^2					
Material: SS 316H with Ni cladding			**Comment:**		
Phenomenon	**Importance Score (Final)**	**Comments**	**Knowledge Level**	**Comments**	**Path Forward**
Chemical Degradation Mechanisms					
Temperature-Gradient Driven Corrosion/deposition	L	Higher impurity levels will exacerbate this phenomenon. Thickness dependent (interdiffusion)			
Galvanic Corrosion	L				
Localized Selective Dissolution	L				
Intergranular Corrosion	L	Thickness and interdiffusion dependent.			
Flow Accelerated Corrosion	L				
High Temperature Oxidation	M	Outside surface	K		
Hydrogen (Tritium) Related Degradation [Hydride formation - embrittlement]	L				
Impurity effect [Fission products, Tritium Fluoride (TF)]	L	Assuming redox control			
Fluorine attack under solidification conditions	L	No solidification expected			
Cladding Interdiffusion	H	Thickness dependent	P		Literature search for interdiffusion data and identify known interdiffusion models. Need validation experiments for different process conditions and temperatures.
Cladding Delamination	H	Dependent on fabrication process and QC	P		Literature search, and get information from Sandvik, Special Metals, WSI welding services, Sumitomo, and Klad. Also look at work from LANL, ORNL, UNLV, Univ. of Florida, and MIT. Review ASTM specification. Review in service examination methods [changes in microstructure over time or radiation effects]. Develop experimental techniques for this material.
Mechanical Degradation Mechanisms					
Thermal Aging	H	Sensitization concerns	K	316H already in ASME code	
Creep	H		P	Known for 316H, but unknown for Ni cladding	Perform long term creep-rupture tests to support the design lifetime. Investigate possible microstructure and property changes for the coupled materials.
Fatigue [LCF, Thermal fatigue] (316H)	M		K	Known for 316H, but unknown for Ni cladding	

Fatigue [LCF, Thermal fatigue] (Ni cladding)	H	Cracking of clad layer will expose shell to molten salt	U	Known for 316H, but unknown for Ni cladding	Perform fatigue tests to develop S-N curves of both nickel and the coupled materials.
Creep-Fatigue	H	Cracking of clad layer will expose shell to molten salt	U	Known for 316H, but unknown for Ni cladding	Perform tests to quantify creep-fatigue interaction of both nickel and coupled materials.
Erosion/Wear	L	Assuming velocities are low			
Crack Growth	H	High for Ni cladding, Moderate for 316H	U	Known for 316H, but unknown for Ni cladding	Literature search. Perform tests to develop creep, fatigue, and creep-fatigue crack growth data. These tests may need to be done for both nickel and coupled materials.
Stress relaxation cracking (SRC)	H	Related to weldment and other fabrication processes.	U	See discussion of weldments	See discussion of weldments
Radiation Degradation Mechanisms					
Irradiation Embrittlement	H	Assuming 10^20 n/cm^2	U	Unknown for Ni	Literature search. Do scoping computational simulations before tests. Perform irradiation tests of coupled material to investigate embrittlement phenomena. Determine embrittlement dose level threshold.
Irradiation Swelling	L	Assuming < 10^20 n/cm^2			
Irradiation Creep	L	Assuming < 10^20 n/cm^2			
Irradiation Assisted Stress Corrosion Cracking/Corrosion fatigue	M	Assuming < 10^20 n/cm^2	U		Literature search. Do scoping computational simulations before tests. Perform irradiation tests of coupled material to investigate irradiation assisted SCC/CF.

Table 2-1c: PIRT table for Vessel and Primary Piping made of Alloy N.

Component: Vessel and Primary Piping					
Environment: 700C steady state, up to 760C transient; 40-60 years; stress levels will vary; 10^20 n/cm^2					
Material: Alloy N			**Comment:** Alloy N does not have adequate creep strength for 40-60 year design.		
Phenomenon	**Importance Score (Final)**	**Comments**	**Knowledge Level**	**Comments**	**Path Forward**
Chemical Degradation Mechanisms					
Temperature-Gradient Driven Corrosion/deposition	H	Higher impurity levels will exacerbate this phenomenon.	K		
Galvanic Corrosion	L				
Localized Selective Dissolution	L	Not including temperature gradient driven dissolution			
Intergranular Corrosion	L				
Flow Accelerated Corrosion	M		P		
High Temperature Oxidation	H	Outside surface	P	MSRE data is available for long term high temperature oxidation in nitrogen with 2-5% oxygen.	Literature search. Generate long term oxidation data in air if needed.
Hydrogen (Tritium) Related Degradation [Hydride formation - embrittlement]	L				
Impurity effect [Fission products, Tritium Fluoride (TF)]	L	Assuming redox control			
Fluorine attack under solidification conditions	L	No solidification expected			
Mechanical Degradation Mechanisms					
Thermal Aging	M		U	Insufficient data for 40-60 years	Literature search. Generate long term thermal aging data for 40-60 year lifetime if needed.
Creep	H		U	Insufficient data for 40-60 years	Perform long term creep-rupture tests to support the design lifetime. Investigate possible microstructure and property changes.
Fatigue [LCF, Thermal fatigue]	H		U	No fatigue curve for Alloy N	Perform fatigue tests to develop S-N curves.
Creep-Fatigue	H		U		Perform tests to quantify creep-fatigue interaction.
Erosion/Wear	M		U		Literature search. Generate erosion data at appropriate velocities and environmental conditions (particles and bubbles).
Crack Growth	H		U		Literature search. Perform tests to develop creep, fatigue, and creep-fatigue crack growth data.
Stress relaxation cracking (SRC)	H	Related to weldment and other fabrication processes.	U		See discussion of weldments

Radiation Degradation Mechanisms					
Irradiation Embrittlement	H	Assuming 10^20 n/cm^2	K	Known from MSRE data	
Irradiation Swelling	L	Assuming < 10^20 n/cm^2			
Irradiation Creep	L	Assuming < 10^20 n/cm^2			
Irradiation Assisted Stress Corrosion Cracking/Corrosion fatigue	M	Assuming < 10^20 n/cm^2	U		Literature search. Do scoping computational simulations before tests. Perform irradiation tests to investigate irradiation assisted SCC/CF.

Table 2-1d: PIRT table for Vessel and Primary Piping made of Alloy N variants.

Component: Vessel and Primary Piping					
Environment: 700C steady state, up to 760C transient; 40-60 years; stress levels will vary; 10^20 n/cm^2					
Material: Alloy N variants			**Comment:** Haynes 242, Haynes 244; ORNL developmental alloys		
Phenomenon	**Importance Score (Final)**	**Comments**	**Knowledge Level**	**Comments**	**Path Forward**
Chemical Degradation Mechanisms					
Temperature-Gradient Driven Corrosion/deposition	H	Higher impurity levels will exacerbate this phenomenon.	U		Evaluate corrosion performance of new materials using isothermal capsule tests. Perform corrosion experiments in thermal-convection loops. Pumped loop testing may be required for down-selected materials.
Galvanic Corrosion	L				
Localized Selective Dissolution	L	Not including temperature gradient driven dissolution			
Intergranular Corrosion	L				
Flow Accelerated Corrosion	L				
High Temperature Oxidation	H	Outside surface	U		Literature search. Generate long term oxidation data in air or the appropriate environment if needed.
Hydrogen (Tritium) Related Degradation [Hydride formation - embrittlement]	L				
Impurity effect [Fission products, Tritium Fluoride (TF)]	L	Assuming redox control			
Fluorine attack under solidification conditions	L	No solidification expected			
Mechanical Degradation Mechanisms					
Thermal Aging	M		U		Literature search. Generate long term thermal aging data for 40-60 year lifetime if needed.
Creep	H		U		Perform long term creep-rupture tests to support the design lifetime. Investigate possible microstructure and property changes.
Fatigue [LCF, Thermal fatigue]	H		U		Perform fatigue tests to develop S-N curves.
Creep-Fatigue	H		U		Perform tests to quantify creep-fatigue interaction.
Erosion/Wear	L	Assuming velocities are low			
Crack Growth	H		U		Literature search. Perform tests to develop creep, fatigue, and creep-fatigue crack growth data.
Stress relaxation cracking (SRC)	H	Related to weldment and other fabrication processes.	U		See discussion of weldments
Radiation Degradation Mechanisms					

Irradiation Embrittlement	H	Assuming 10^20 n/cm^2	U		Literature search. Do scoping computational simulations before tests. Perform irradiation tests to investigate embrittlement phenomena. Determine embrittlement dose level threshold.
Irradiation Swelling	L	Assuming < 10^20 n/cm^2			
Irradiation Creep	L	Assuming < 10^20 n/cm^2			
Irradiation Assisted Stress Corrosion Cracking/Corrosion fatigue	M	Assuming < 10^20 n/cm^2	U		Literature search. Do scoping computational simulations before tests. Perform irradiation tests to investigate irradiation assisted SCC/CF.

2.2. Primary Heat Exchanger

Table 2-2a: PIRT table for Primary Heat Exchanger made of Alloy N.

Component: Primary Heat Exchanger					
Environment: 700C steady state, up to 760C transient; 40-60 years; stress levels will vary; replaceable, FLiBe and FLiNaK					
Material: Alloy N			**Comment:** Must be replaceable item if using Alloy N.		
Phenomenon	**Importance Score (Final)**	**Comments**	**Knowledge Level**	**Comments**	**Path Forward**
Chemical Degradation Mechanisms					
Temperature-Gradient Driven Corrosion/deposition	H	Higher impurity levels will exacerbate this phenomenon.	K		
Galvanic Corrosion	L				
Localized Selective Dissolution	L	Not including temperature gradient driven dissolution			
Intergranular Corrosion	L				
Flow Accelerated Corrosion	M		P	Loop test results available from MSRE reports.	Literature search, specifically of MSRE heat exchangers. Perform scaled heat exchanger loop tests.
High Temperature Oxidation	H	External surface of shell	P		Literature search. Generate long term oxidation data in air if needed.
Hydrogen (Tritium) Related Degradation [Hydride formation - embrittlement]	L				
Impurity effect [Fission products, Tritium Fluoride (TF)]	L	Assuming redox control			
Fluorine attack under solidification conditions	L	No solidification expected			
Mechanical Degradation Mechanisms					
Thermal Aging	M		U	New data generation requirement is less than for 40-60 year case	Literature search. Generate long term thermal aging data for 40-60 year lifetime if needed.
Creep	H		U	New data generation requirement is less than for 40-60 year case	Perform long term creep-rupture tests to support the design lifetime. Investigate possible microstructure and property changes.
Fatigue [LCF, Thermal fatigue]	H		U	New data generation requirement is less than for 40-60 year case	Perform fatigue tests to develop S-N curves.

Creep-Fatigue	H		U	New data generation requirement is less than for 40-60 year case	Perform tests to quantify creep-fatigue interaction.
Erosion/Wear	M	Assuming velocities are moderate and thin wall tubing.	U		Literature search, specifically of MSRE heat exchangers. Perform scaled heat exchanger loop tests.
Fretting Wear	H	Caused by flow induced vibrations.	U		Literature search, specifically of MSRE heat exchangers. Perform scaled heat exchanger loop tests.
Crack Growth	H		U	New data generation requirement is less than for 40-60 year case	Literature search. Perform tests to develop creep, fatigue, and creep-fatigue crack growth data.
Radiation Degradation Mechanisms					
Irradiation Embrittlement	L				
Irradiation Swelling	L				
Irradiation Creep	L				
Irradiation Assisted Stress Corrosion Cracking/Corrosion fatigue	L				

Table 2-2b: PIRT table for Primary Heat Exchanger made of Alloy N variants.

Component: Primary Heat Exchanger					
Environment: 700C steady state, up to 760C transient; 40-60 years; stress levels will vary; replaceable, FLiBe and FLiNaK					
Material: Alloy N variants				**Comment:** Targeting non-replaceable heat exchanger components; Better mechanical properties and equivalent corrosion performance.	
Phenomenon	**Importance Score (Final)**	**Comments**	**Knowledge Level**	**Comments**	**Path Forward**
Chemical Degradation Mechanisms					
Temperature-Gradient Driven Corrosion/deposition	H	Higher impurity levels will exacerbate this phenomenon.	U		Evaluate corrosion performance of new materials using isothermal capsule tests. Perform corrosion experiments in thermal-convection loops. Pumped loop testing may be required for down-selected materials.
Galvanic Corrosion	L				
Localized Selective Dissolution	L	Not including temperature gradient driven dissolution			
Intergranular Corrosion	L				
Flow Accelerated Corrosion	M		U		Literature search, specifically of MSRE heat exchangers. Perform scaled heat exchanger loop tests.
High Temperature Oxidation	H	External surface of shell	U		Literature search. Generate long term oxidation data in air if needed.
Hydrogen (Tritium) Related Degradation [Hydride formation - embrittlement]	L				
Impurity effect [Fission products, Tritium Fluoride (TF)]	L	Assuming redox control			
Fluorine attack under solidification conditions	L	No solidification expected			
Mechanical Degradation Mechanisms					
Thermal Aging	M		U		Literature search. Generate long term thermal aging data for 40-60 year lifetime if needed.
Creep	H		U		Perform long term creep-rupture tests to support the design lifetime. Investigate possible microstructure and property changes.
Fatigue [LCF, Thermal fatigue]	H		U		Perform fatigue tests to develop S-N curves.
Creep-Fatigue	H		U		Perform tests to quantify creep-fatigue interaction.
Erosion/Wear	M	Assuming velocities are moderate and thin wall tubing.	U		Literature search, specifically of MSRE heat exchangers. Perform scaled heat exchanger loop tests.
Fretting Wear	H		U		Literature search, specifically of MSRE heat exchangers. Perform scaled heat exchanger loop tests.
Crack Growth	H		U		Literature search. Perform tests to develop creep, fatigue, and creep-fatigue crack growth data.
Radiation Degradation Mechanisms					
Irradiation Embrittlement	L				
Irradiation Swelling	L				
Irradiation Creep	L				

Irradiation Assisted Stress Corrosion Cracking/Corrosion fatigue	L				

2.3. Steam Generator Tubes

Table 2-3: PIRT table for Steam Generator Tubes made of Alloy 800-H with Alloy N cladding.

Component: Steam Generator Tubes					
Environment: 650C steady state, up to 715C transient; 40-60 years; 24MPa; FLiNaK inside and supercritical steam outside					
Material: Alloy 800-H with Alloy N cladding inside			**Comment:** Manufacturing issues must be resolved; welding issues must be resolved.		
Phenomenon	**Importance Score (Final)**	**Comments**	**Knowledge Level**	**Comments**	**Path Forward**
Chemical Degradation Mechanisms					
Temperature-Gradient Driven Corrosion/deposition	L	Only deposition expected			
Galvanic Corrosion	L				
Localized Selective Dissolution	L				
Intergranular Corrosion	L	Thickness and interdiffusion dependent.			
Flow Accelerated Corrosion	L				
High Temperature Oxidation	M	Steam side	K		
Hydrogen (Tritium) Related Degradation [Hydride formation - embrittlement]	L				
Impurity effect [Fission products, Tritium Fluoride (TF)]	L	Assuming redox control. Very low tritium or fission products expected.			
Fluorine attack under solidification conditions	L	No solidification expected			
Cladding Interdiffusion	H	Lower temperatures, but thinner layer	P		Literature search for interdiffusion data and identify known interdiffusion models. Need validation experiments for different process conditions and temperatures. This issue has higher importance because tubes are thin.
Cladding Delamination	H	Dependent on fabrication process and QC	P		Literature search, and get information from Sandvik, Special Metals, WSI welding services, Sumitomo, and Klad. Also look at work from LANL, ORNL, UNLV, Univ. of Florida, and MIT. Review ASTM specification. Review in service examination methods [changes in microstructure over time]. Develop experimental techniques for this material.
Mechanical Degradation Mechanisms					
Thermal Aging	M		K	Alloy 800-H already in ASME code; Aging data for Alloy N not available.	
Creep	H	Cracking of clad layer will expose base metal to molten salt	P	Known for 800-H, but unknown	Perform long term creep-rupture tests to support the design lifetime. Investigate possible microstructure and property changes for the coupled

				for Alloy N cladding	materials. Interdiffusion effects will be magnified due to thin cross section of tubes. Microstructure, especially grain size may be different from bulk material.
Fatigue [LCF, Thermal fatigue] (800-H)	M	Cracking of clad layer will expose base metal to molten salt	K	Known for 800-H, but unknown for Alloy N cladding	
Fatigue [LCF, Thermal fatigue] (Alloy N cladding)	H	Cracking of clad layer will expose base metal to molten salt	U	Known for 800-H, but unknown for Alloy N cladding	Perform fatigue tests to develop S-N curves of both Alloy N and the coupled materials. Interdiffusion effects will be magnified due to thin cross section of tubes. Microstructure, especially grain size may be different from bulk material.
Creep-Fatigue	H	Cracking of clad layer will expose base metal to molten salt	U	Known for 800-H, but unknown for Alloy N cladding	Perform tests to quantify creep-fatigue interaction of both Alloy N and coupled materials. Interdiffusion effects will be magnified due to thin cross section of tubes. Microstructure, especially grain size may be different from bulk material.
Erosion/Wear	M	Assuming velocities are moderate and thin wall tubing.	U		Literature search. Perform scaled steam generator loop tests.
Fretting Wear	H	Only Alloy 800-H	P		Literature search. Perform scaled steam generator loop tests.
Crack Growth	H	High for Alloy N cladding, Moderate for Alloy 800-H	U	Maybe known for 800-H, but unknown for Alloy N cladding	Literature search. Perform tests to develop creep, fatigue, and creep-fatigue crack growth data. These tests may need to be done for both Alloy N and coupled materials. Interdiffusion effects will be magnified due to thin cross section of tubes. Microstructure, especially grain size may be different from bulk material.
Stress relaxation cracking (SRC)	H	Can be high for Alloy 800-H. Related to weldment and other fabrication processes.	K		
Radiation Degradation Mechanisms					
Irradiation Embrittlement	L				
Irradiation Swelling	L				
Irradiation Creep	L				
Irradiation Assisted Stress Corrosion Cracking/Corrosion fatigue	L				

2.4. Steam Generator Vessel

Table 2-4: PIRT table for Steam Generator Vessel made of Alloy 800-H.

Component: Steam Generator Vessel					
Environment: 650C steady state, up to 715C transient; 40-60 years; 24MPa; supercritical steam					
Material: Alloy 800-H				**Comment:** Manufacturing issues must be resolved; welding issues must be resolved.	
Phenomenon	**Importance Score (Final)**	**Comments**	**Knowledge Level**	**Comments**	**Path Forward**

Chemical Degradation Mechanisms					
Air side High Temperature Oxidation	H		K		
Water side high temperature oxidation	H	Water chemistry control is critical	K		
Stress corrosion cracking (SCC)	H	Water chemistry control is critical	K		
Corrosion Fatigue	L				
Mechanical Degradation Mechanisms					
Thermal Aging	M		K	Alloy 800-H already in ASME code	
Creep	H		K	Alloy 800-H already in ASME code	
Fatigue [LCF, Thermal fatigue] (800-H)	M		K	Alloy 800-H already in ASME code	
Creep-Fatigue	H		K	Alloy 800-H already in ASME code	
Erosion/Wear	L				
Fretting Wear	L				
Crack Growth	M	Moderate for Alloy 800-H	K	Maybe known for 800-H	
Stress relaxation cracking (SRC)	H	Can be high for Alloy 800-H. Related to weldment and other fabrication processes.	K		
Thermal Aging	M		K	Alloy 800-H already in ASME code	
Radiation Degradation Mechanisms					
Irradiation Embrittlement	L				
Irradiation Swelling	L				
Irradiation Creep	L				
Irradiation Assisted Stress Corrosion Cracking/Corrosion fatigue	L				

2.5. Intermediate Loop Piping

Table 2-5: PIRT table for Intermediate Loop Piping made of Alloy N.

Component: Intermediate Loop Piping					
Environment: ≤675C steady state, up to 735C transient; 40-60 years; ??? stress level-FLiNaK(inside) and air(outside)					
Material: Alloy N				**Comment:** Must be replaceable if using Alloy N	
Phenomenon	**Importance Score (Final)**	**Comments**	**Knowledge Level**	**Comments**	**Path Forward**
Chemical Degradation Mechanisms					
Temperature-Gradient Driven Corrosion/deposition	M	Higher impurity levels will exacerbate this phenomenon.	K		
Galvanic Corrosion	L				
Localized Selective Dissolution	L	Not including temperature gradient driven dissolution			
Intergranular Corrosion	L				
Flow Accelerated Corrosion	M		P		
High Temperature Oxidation	H	External surface of pipe	P		Literature search. Generate long term oxidation data in air if needed.
Hydrogen (Tritium) Related Degradation [Hydride formation - embrittlement]	L				
Impurity effect [Fission products, Tritium Fluoride (TF)]	L	Assuming redox control in FLiNaK			
Fluorine attack under solidification conditions	L	No solidification expected			
Mechanical Degradation Mechanisms					
Thermal Aging	M		U	New data generation requirement is less than for 40-60 year case	Literature search. Generate long term thermal aging data for 40-60 year lifetime if needed.
Creep	H		U	New data generation requirement is less than for 40-60 year case	Perform long term creep-rupture tests to support the design lifetime. Investigate possible microstructure and property changes.
Fatigue [LCF, Thermal fatigue]	H		U	New data generation requirement is less than for 40-60 year case	Perform fatigue tests to develop S-N curves.
Creep-Fatigue	H		U	New data generation	Perform tests to quantify creep-fatigue interaction.

				requirement is less than for 40-60 year case	
Erosion/Wear	M	Assuming velocities are moderate	U		Literature search. Generate erosion data at appropriate velocities and environmental conditions (particles and bubbles).
Fretting wear	L				
Crack Growth	H		U	New data generation requirement is less than for 40-60 year case	Literature search. Perform tests to develop creep, fatigue, and creep-fatigue crack growth data.
Stress relaxation cracking (SRC)	H	Related to weldment and other fabrication processes.	U		See discussion of weldments
Radiation Degradation Mechanisms					
Irradiation Embrittlement	L				
Irradiation Swelling	L				
Irradiation Creep	L				
Irradiation Assisted Stress Corrosion Cracking/Corrosion fatigue	L				

2.6. Valves and Pumps

Table 2-6a: PIRT table for Valves and Pumps made of Alloy N and variants.

Component: Valves and Pumps					
Environment: 700C steady state, up to 760C transient; 40-60 years; ??? stress level; wear resistance					
Materials: Alloy N and variants				**Comment:** Alloy N and variants for the wetted surface. Alloy N does not have adequate creep strength for 40-60 year design. Look at corrosion and wear resistant coatings as well.	
Phenomenon	**Importance Score (Final)**	**Comments**	**Knowledge Level**	**Comments**	**Path Forward**
Chemical Degradation Mechanisms					
Temperature-Gradient Driven Corrosion/deposition	L	Assuming pump is on the cold side			
Galvanic Corrosion	L				
Localized Selective Dissolution	L	Not including temperature gradient driven dissolution			
Intergranular Corrosion	L				

Flow Accelerated Corrosion	M		U		Literature search. Generate data for appropiate velocities related to pumps and valves.
High Temperature Oxidation	L	Pump manufacture should select material for high temp oxidation resistance for air exposed surfaces			
Hydrogen (Tritium) Related Degradation [Hydride formation - embrittlement]	L				
Impurities effect [Fission products, Tritium Fluoride (TF)]	L	Assuming redox control as well as the impurities can be effectively removed			
Fluorine attack under solidification conditions	L	No solidification expected			
Mechanical Degradation Mechanisms					
Thermal Aging	M		U	Insufficient data for 40-60 years	Literature search. Generate long term thermal aging data for 40-60 year lifetime if needed.
Creep	H		U	Insufficient data for 40-60 years	Perform long term creep-rupture tests to support the design lifetime. Investigate possible microstructure and property changes.
Fatigue [LCF, Thermal fatigue]	H		U	No fatigue curve for Alloy N	Perform fatigue tests to develop S-N curves.
Creep-Fatigue	H		U		Perform tests to quantify creep-fatigue interaction.
Erosion/Wear/Cavitation	L	Assuming velocities are low and pressure drop is low			
Crack Growth	H		U		Literature search. Perform tests to develop creep, fatigue, and creep-fatigue crack growth data.
Stress relaxation cracking (SRC)	L	related to fabrication processes			
Radiation Degradation Mechanisms					
Irradiation Embrittlement	L				
Irradiation Swelling	L				
Irradiation Creep	L				
Irradiation Assisted Stress Corrosion Cracking/Corrosion fatigue	L				

Table 2-6b: PIRT table for Valve and Pump seal materials.

Component: Valves and Pumps					
Environment: 700C steady state, up to 760C transient; 40-60 years; ??? stress level; wear resistance					
Materials: Boron Nitride (seals) and SiC (seals)			**Comment:**		
Phenomenon	**Importance Score (Final)**	**Comments**	**Knowledge Level**	**Comments**	**Path Forward**
Chemical Degradation Mechanisms					
Temperature-Gradient Driven Corrosion/deposition	L				
Galvanic Corrosion	L				
Localized Selective Dissolution	L				
Intergranular Corrosion	L				
Flow Accelerated Corrosion	L				
High Temperature Oxidation	L	Need more data for 650C			
Hydrogen (Tritium) Related Degradation [Hydride formation - embrittlement]	L				
Impurities effect [Fission products, Tritium Fluoride (TF)]	M	Assuming redox control as well as the impurities can be effectively removed	U	No data available	Literature search. Look at MSRE experience and Kevin Robb's report on pumps. Generate impurity effect data for candidate materials.
Fluorine attack under solidification conditions	L	No solidification expected			
Mechanical Degradation Mechanisms					
Thermal Aging	L				
Creep	L				
Fatigue [LCF, Thermal Shock]	H		U	No data available	Literature search. Look at MSRE experience and Kevin Robb's report on pumps. Generate fatigue data for candidate materials.
Creep-Fatigue	L				
Erosion/Wear/Cavitation	H		U	No data available	Literature search. Look at MSRE experience and Kevin Robb's report on pumps. Generate erosion/wear/cavitation for candidate materials at the appropriate velocities and environmental conditions.
Crack Growth	L	For composites it is design/architecture dependent			
Stress relaxation cracking (SRC)	L				
Radiation Degradation Mechanisms					
Irradiation Embrittlement	L				
Irradiation Swelling	L				
Irradiation Creep	L				
Irradiation Assisted Stress Corrosion Cracking/Corrosion fatigue	L				

2.7. Welds

Table 2-7: PIRT table for Welds.

Component: Welds		
Environment: FLiBe and FLiNaK		
Comment on Importance: Microstructure and alloy composition may be different from base materials considered. Properties may depend on post-weld heat treatment.		
Base Material	**Comment on Knowledge Level**	**Path Forward**
Alloy N	Alloy N welding procedures for gas tungsten arc (GTA) welds were developed for the MSRE. Corrosion performance of Alloy N welds was demonstrated to be successful in operating systems, however this information may not be retrievable. Brazing procedures were developed for heat exchangers. Welding procedures for commercial Alloy N are available.	If data cannot be retrieved, corrosion tests of Alloy N welds must be performed. SINAP is developing Alloy N welding procedures for large components.
Alloy N Variants	Unknown	Welding procedures for Alloy N variants must be developed. Corrosion tests of welds must be performed.
Bimetallic Materials	Unknown	Welding procedures for bimetallic materials must be developed. Discuss with Special Metals the techniques they developed for welding co-extruded tubes. Need to investigate other joining and fabrication methods. Apply additive manufacturing technology for graded coatings and heat exchangers. Mechanical testing of additively manufactured materials must be performed. Corrosion tests of welds and additively manufactured materials must be performed.

2.8. Other Important Factors in Material Degradation in FHR Environments and its Control

Table 2-8: Other important factors in material degradation in FHR environments and its control.

Impurity control and property measurement are important.
Electrochemical measurement techniques must be created/recreated.
Measurement of source terms in salt to detect fuel failure. (Gamma spectroscopy?)
Chemical measurement methods of low level impurities must be developed.
Correlations between low level impurity content and corrosion must be created.
Chemical form of fission products in the salt environment must be determined. Fission products may not only exist as fluorides.
Need to determine salt impurity level at startup of reactor.

3. Review of the AHTR Conceptual Design

In preparation for a previous PIRT panel on neutronics in Dec. 2015, a whitepaper was prepared (Rahnema et al. 2015) which also incorporated a definition of a reference AHTR primary system and core design, for benchmarking purposes. This whitepaper also listed information on the materials selected for their benchmark FHR design. We have used the same design information (with author's permission) for this whitepaper to be consistent with other related FHR-PIRT like activities. The design presented here is not final but is just a starting point for discussion on selection of materials and their possible degradation mechanisms. A definition of all geometric and material properties for this design was based on work from ORNL and other related projects over the last 10+ years. The general design of the AHTR is presented in two ORNL reports; both reports use slightly different numbers for specific design parameters, because the most recent design has been partially optimized. (Holcomb, et al., 2011) (Varma, et al., 2012) . More recent information on the essential design elements and material selection for FHR is also reviewed in section 5 of a 2013 ORNL report on FHR development roadmap (Holcomb, et al., 2013). Details of this benchmark FHR design are described in next sections.

3.1. General Overview of the Plant Design

Following are the design parameters used for the benchmark AHTR design considered for the neutonics PIRT (Farzad et al. 2015). This design is not optimized but can help with the understanding of environmental and physical conditions to be experienced by the selected materials for different FHR components. Materials described or selected for this design (highlighted and "underlined and bold" fonts in the following sections) are not always with optimum properties from their corrosion resistance, but will provide some guideline for the selection of an appropriate material later. New alloys are still being developed or optimized for the FHR environments.

The Advanced High-Temperature Reactor (AHTR) was designed to have a power of 3400 MW_{th} and an efficiency of approximately 45%, corresponding to a power of 1530 MW_e. The AHTR design concept is a Fluoride High-Temperature Reactor (FHR) with a primary coolant of FLiBe ($2LiF\text{-}BeF_2$), coupled to an intermediary salt loop containing $KF\text{-}ZrF_4$. The power cycle is based on the supercritical water cycle, with the water loop coupled to the intermediary salt loop. The AHTR exploits passive safety systems, such as Direct Reactor Auxiliary Cooling System (DRACS), in order to minimize the requirements for external support during accident scenarios. A general plant overview is presented in Figure 3-1.

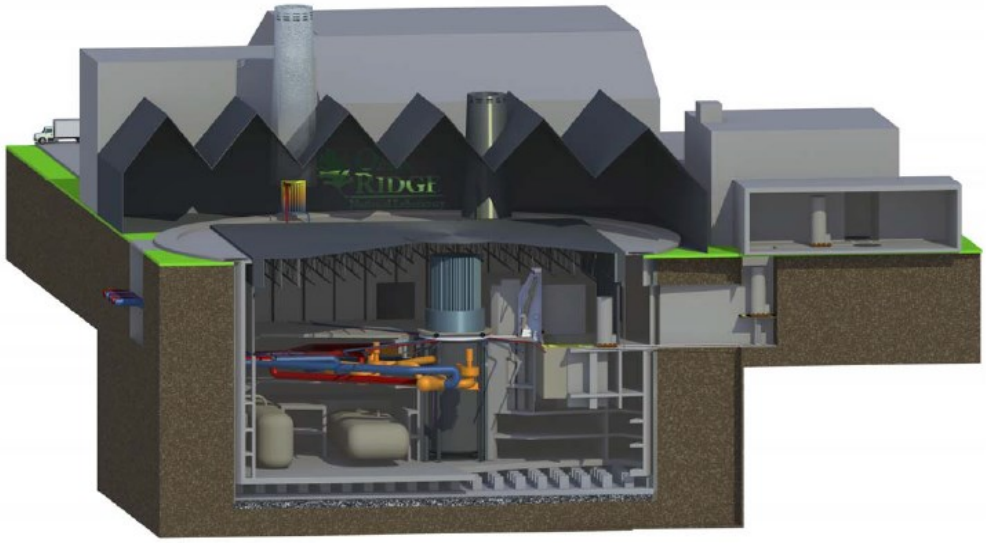

Figure 3-1: Overview of the AHTR plant design. (Varma, et al., 2012)

The reactor fuel is based on the Tristructural-Isotropic (TRISO) particles and is in the form of a layered uranium oxy-carbide (UCO) material. The most recent design from ORNL calls for a fuel enrichment of 9 wt%, though an enrichment of 19.75 wt% was called for in the original preconceptual design. (Holcomb, et al., 2011) (Varma, et al., 2012) The core consists of these TRISO particles loaded into 252 active fuel assemblies containing 18 fuel plates each, arranges such that the assembly is hexagonal. The active height of the AHTR core is 5.5 m and utilizes graphite for both moderation and reflection of neutrons.

The primary reactor coolant salt is FLiBe, which undergoes a temperature increase of 50°C on average, across the core (including the bypass flow). The core inlet temperature is 650°C and the outlet is 700°C. From the design parameters, one can calculate the mass flow rate of FLiBe (assuming the average specific heat of the coolant is 2,415 J/kg·K) to be approximately 28,150 kg/s. The reactor vessel is not pressurized.

Table 3-1: General AHTR plant parameters.

Parameter	Value	Units
Core Thermal Power	3,400	MW
Overall Thermal Efficiency	45%	-
Fuel Type	TRISO	-
Uranium Composition	UCO	-
Number of Fuel Assemblies	252	-
Moderator and Reflector Material	**Graphite**	-
Active Core Height	5.5	m
Primary Coolant Salt	FLiBe	-
Core Inlet Temperature	650	°C

Core Outlet Temperature	700	°C

Further details on the core specifications will be provided in the subsequent sections of this document. Additionally, general information about the intermediate salt loop, power cycle, and decay heat removal system can be found in the ORNL preconceptual/conceptual design documents. (Holcomb, et al., 2011) (Varma, et al., 2012)

3.2. Reactor Vessel and Out-of-Core Structure

This section describes the AHTR reactor vessel and some components of the out-of-core structure. The reactor vessel is roughly cylindrical in nature and hung from its upper flange, to minimize the stress incurred by the thermal expansion. (Varma, et al., 2012) Figure 3-2 depicts the basic overview of the AHTR vessel and core location.

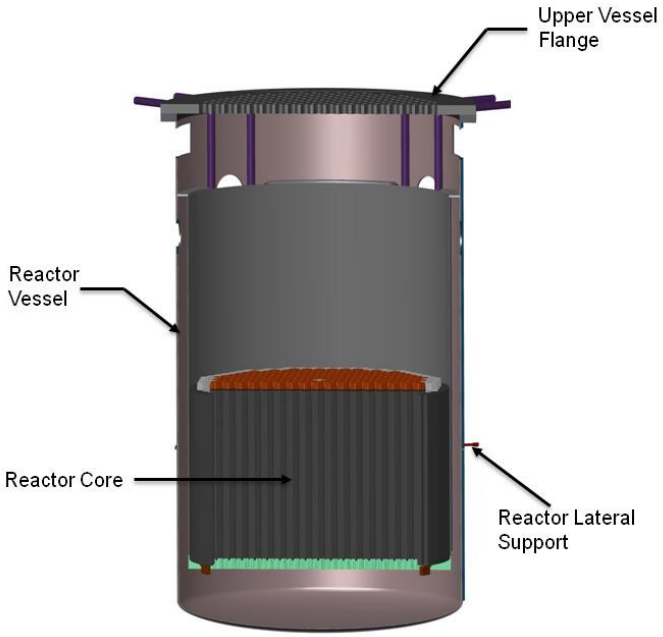

Figure 3-2: AHTR reactor vessel cross section. (Varma, et al., 2012)

Table 3-2 provides the global parameters of the AHTR reactor vessel, which is made from 800-H alloy and has a yield strength of 20 MPa at 700°C. There is a possibility of corrosion with the FLiBe coolant and the **800-H alloy**, thus a thin (1 cm thick) liner of **Alloy-N** is included on surfaces contacting the FLiBe. The vessel thickness is not defined in the ORNL reference reports. However, it is assumed to be 5 cm, though from a mechanical standpoint a larger thickness may be required.

Table 3-2: Global parameters of the AHTR reactor vessel.

Parameter	Value	Units
Exterior Vessel Diameter	10.5	m
Vessel Height	19.1	m
Primary Salt Depth Above Upper Support Plate	7.15	m
Primary Piping Interior Diameter	1.24	m
Number of DRACS	3	-
Core Barrel Material	**C-C Composite**	-
Vessel and Primary Piping Material	**800-H Alloy w/Alloy-N Lining**	-

The full reactor vessel configuration can be observed in Figure 3-3, which also depicts the location of the refueling lobe. The vessel size exceeds the limits for transportation by rail, thus the vessel must be transported to the site in sections and welded into the final vessel. (Varma, et al., 2012)

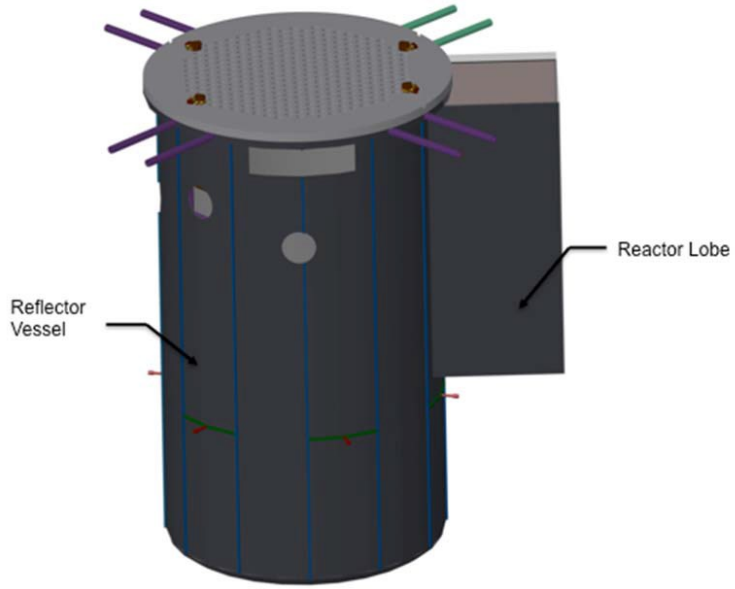

Figure 3-3: AHTR reactor vessel. (Varma, et al., 2012)

3.2.1. **Upper Plenum**

The upper plenum is delimited by the upper support plate and the reactor vessel flange. The upper portion of the plenum is filled with Argon cover gas (not pressurized) at a temperature of 250°C. The cover gas volume has a height of 3.19 m. The lower portion of the upper plenum (Figure 3-4) is filled with FLiBe coming from the core, at an average temperature of 700°C. The salt is 7.15 m deep from the upper core plate. During normal

operation, guide tubes for leader rods occupy the upper plenum. These rods are retractable, in order to provide access for refueling.

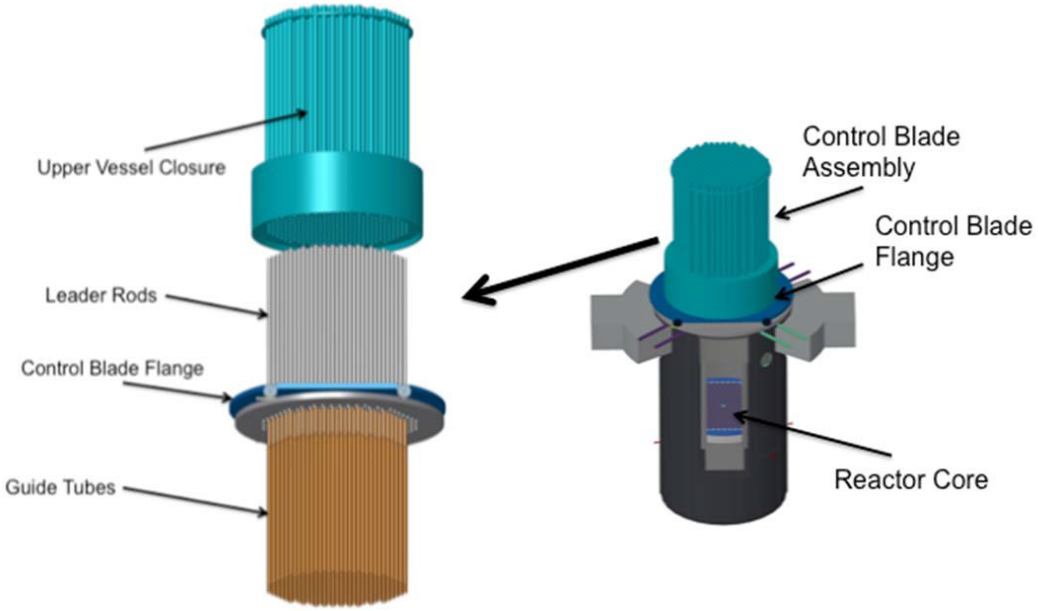

Figure 3-4: AHTR upper plenum, guide tubes, and the upper vessel closure. (Varma, et al., 2012)

3.2.2. **Top Flange**

The top flange (Figure 3-5) has a diameter of 11.6 m and a thickness of 35 cm, consisting of a truss structure fabricated by two 1.5 cm thick **stainless steel top** and bottom plates (to reduce weight). The volume fraction of the solid material is 13.45% of a reference cylinder that wraps the flange. The flange is maintained at a temperature of 250°C by the Argon gas in the upper portion of the upper plenum.

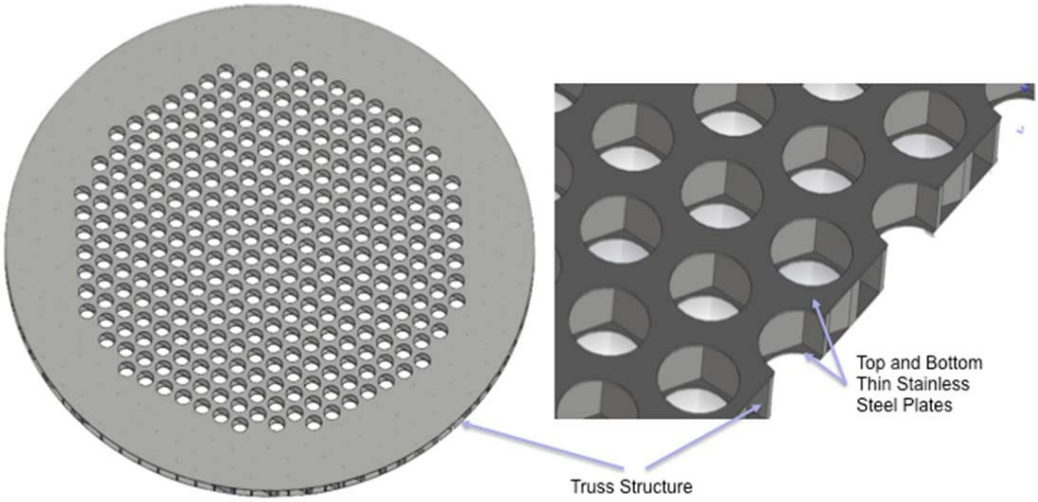

Figure 3-5: AHTR top flange configuration. (Varma, et al., 2012)

3.3. Core Barrel and Downcomer

The core barrel separates the core from the downcomer/DRACS heat exchanger region and is made up of a 2 cm thick **Carbon-Carbon (C-C) composite**. The interior face (towards the core) of the barrel has a thin plating of **boron carbide** (thickness 1 cm), which attenuates neutron radiation before it impacts the reactor vessel. The internal diameter of the core barrel is 9.56 m and the outer diameter is 9.62 m, resulting in a core barrel that is 6 cm thick. The operating temperature is 650°C (same as inlet core temperature) and flow direction is downward in the downcomer region (upward in the core). The downcomer region is subdivided azimuthally into 8 angular zones; 3 downcomer sections, 3 DRACS sections, 1 maintenance cooling system, and a 1 refueling lobe. Figure 3-6 depicts the core barrel and downcomer regions of the AHTR.

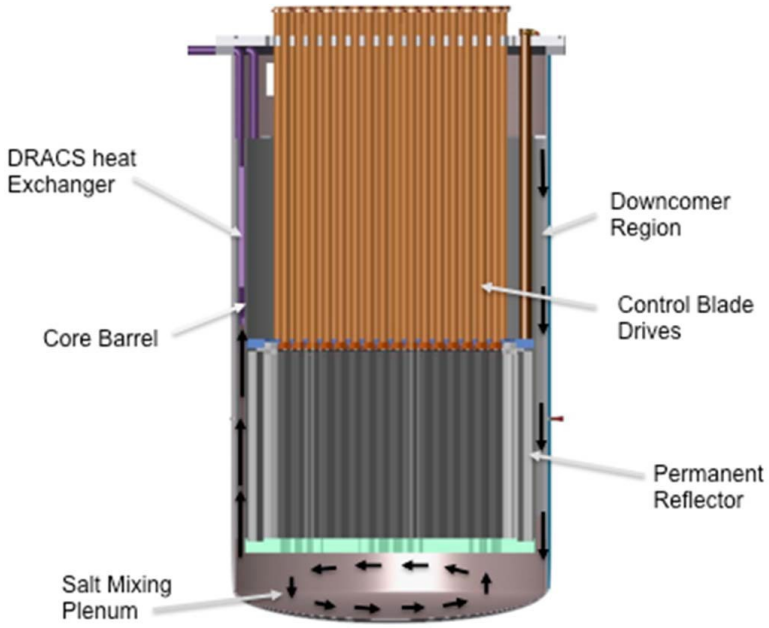

Figure 3-6: Vertical cross section of the AHTR reactor vessel and core, showing the downcomer region and core barrel. (Varma, et al., 2012)

3.4. Reactor Core

The reactor core contains 252 fuel assemblies arranged hexagonally. The central assembly is not fueled, but serves as a moderator block **(it has the same composition and structure as the outer removable reflector blocks)**. The gap between assemblies is 1.8 cm and the equivalent diameter of the reactor core is 7.81 m for the fueled part. One ring of replaceable reflector assemblies surrounds the last ring of fueled assemblies, and then a permanent reflector completes the core. The equivalent diameter of the core including the replaceable reflector is 8.69 m. The outer radius of the permanent reflector is 9.56 m. The core height is 6 m, of which 5.5 m is the active core; top and bottom nozzle/reflector regions are 25 cm each, the support plates are 35 cm thick, resulting in an overall height of 6.7 m for the core and support plates. Figure 3-7 provides a view of the core reflectors, upper support plate and lower support plate. Figure 3-8 depicts a horizontal cross section of the core through the fuel midplane.

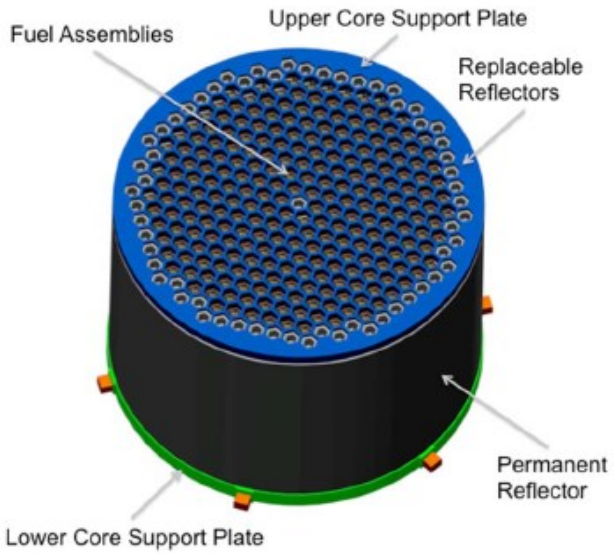

Figure 3-7: AHTR core reflector, upper support plate, and lower support plate. (Varma, et al., 2012)

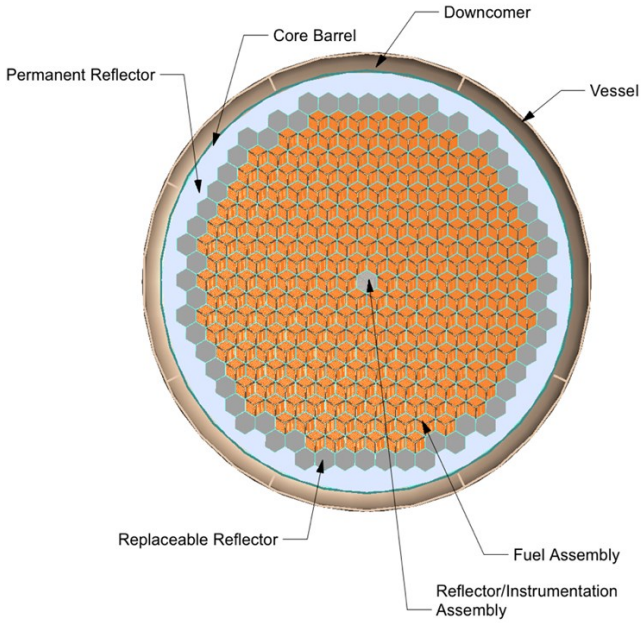

Figure 3-8: AHTR core horizontal cross section through fuel midplane. (Varma, et al., 2012)

3.4.1. **Replaceable Reflector**

The replaceable reflector surrounds the outermost fuel assembly ring and consists of a single ring of removable reflector blocks (shown as dark gray in Figure 3-8). The replaceable reflector blocks are made of **graphite** and have the same size and shape as the fueled assemblies. In the reference design, they are not provided with control rods. However, in principle a control rod could be added to each reflector block to facilitate the

control of the reactor power. No coolant channels are present in the reflector block, but they could be added if cooling is required.

3.4.2. Permanent Reflector

The permanent reflector surrounds the removable reflector ring and consists of **solid graphite** sections (depicted as light grey in Figure 3-8). Its shape conforms to the replaceable reflector blocks on the inner side and has a cylindrical outer shape that conforms to the core barrel.

3.4.3. Lower Support Plate

The lower support plate provides support to the core and reflector. It is a honeycomb structure that is attached to the reactor vessel through lateral junctions. The lower support plate is made of **SiC-SiC composite** and is 35 cm thick. Channel cuts have been made in the lower plate to direct the flow of FLiBe into the fuel assemblies (Figure 3-9). Additionally, indexing holes and guides provide for proper alignment of fuel assemblies during refueling operations.

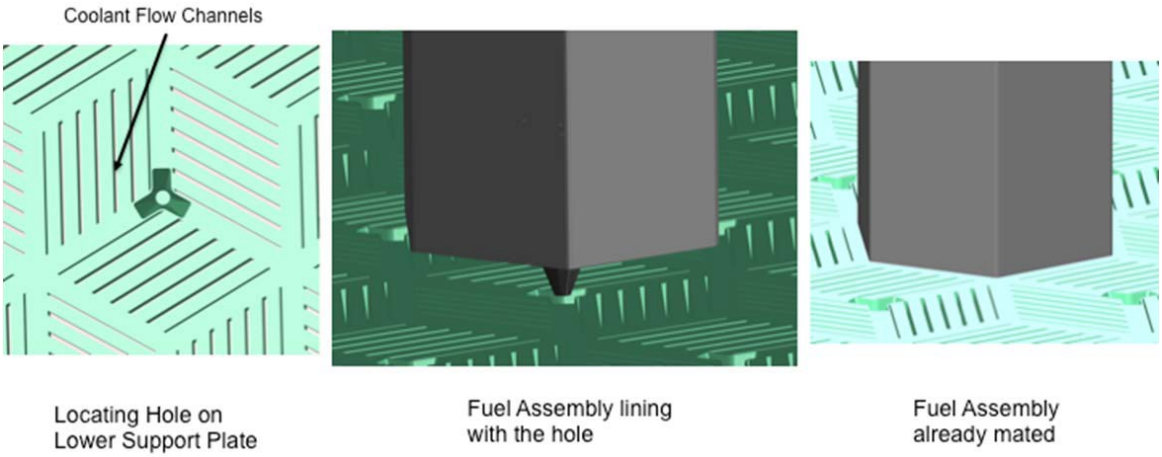

Figure 3-9: Detailed representation of the AHTR lower support plate. (Varma, et al., 2012)

For neutronics modeling purposes, as a simplified model of the lower support plate can be represented by a cylinder of the same dimensions made of 14.96% FLiBe and 85.04% **graphite**, by volume at a temperature of 650°C.

3.4.4. Upper Support Plate

The upper support plate's primary function is to hold core components in place, against the upward flowing salt. The upper support plate is 35 cm thick and made of a **SiC-SiC composite** (same material as the lower support plate). Four drive rods are used to raise and lower the upper support plate during refueling outages. Figure 3-10 depicts the

location of the upper support plate and the location of the drive rods in the salt filed portion of the upper plenum.

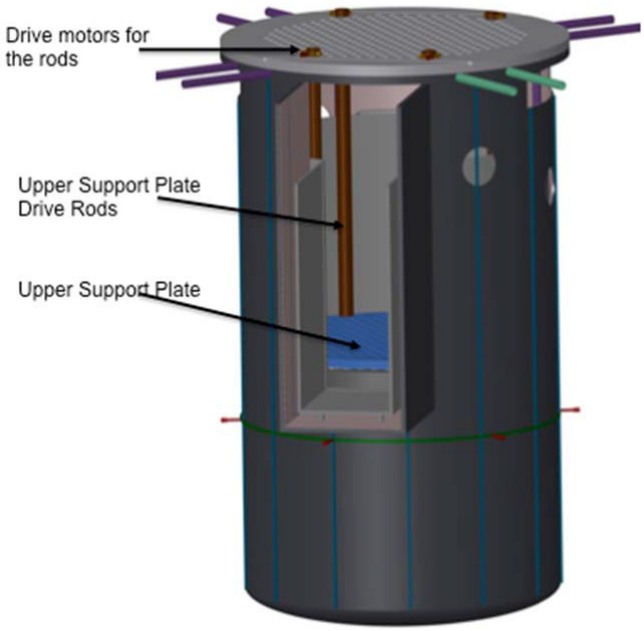

Figure 3-10: View of the salt filled portion of the upper plenum and the drive rods for the upper support plate. (Varma, et al., 2012)

The upper support plate makes tangential contact with the hemispherical contacts on the grappling collar of the fuel assemblies (Figure 3-11). The webbing on the upper core support plate fills the inter-assembly gap and provides a reduction in flow vibrations. For neutronics modeling purposes, as a simplified model of the upper support plate can be represented by a cylinder of the same dimensions made of 78.9% FLiBe and 21.1% **graphite**, by volume at a temperature of 700°C.

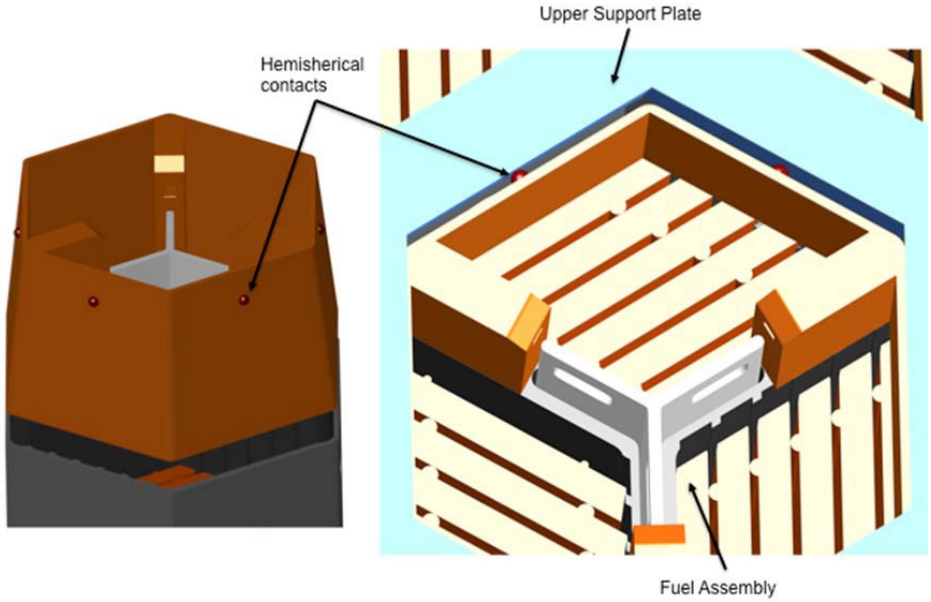

Figure 3-11: Contact between the AHTR fuel assembly grappling collar and the upper support plate. (Varma, et al., 2012)

3.4.5. **Consolidated AHTR Core and Vessel Dimensions**

This section provides a consolidated placement of the overall dimensions of the major components in the AHTR vessel and core. Some parameters have been assumed, since they are not fully specified in the ORNL preconceptual AHTR design description. Table 3-3 provides the outer diameters (OD) of the various vessel components. The following assumptions were made in preparation of these dimensions:

- The height of the lower plenum is assumed to be 2 m; this results in a cover gas volume height of 3.19 m. Increasing the lower plenum height results in a decreased cover gas volume height in the upper plenum.
- The reactor vessel thickness is 5 cm, plus a 1 cm **Alloy-N** liner.
- The height of the downcomer (with respect to the lower face of the lower support plate, corresponding to the top of the lower plenum) is assumed to be 13 m.

Table 3-3: AHTR vessel and core component outer diameters (OD). (Varma, et al., 2012)

Parameter	Value	Units
Core OD	7.81	m
Replaceable Reflector Equivalent OD	8.69	m
Permanent Reflector Equivalent OD	9.56	m
Boron Layer OD	9.58	m
Barrel OD	9.62	m
Downcomer OD	10.38	m
Alloy-N Liner OD	10.40	m
Vessel OD	10.50	m

Figure 3-12 presents the major vessel and core dimensions, while Figure 3-13 and Figure 3-14 provide an enhanced view of the top of the downcomer and top of the core, respectively.

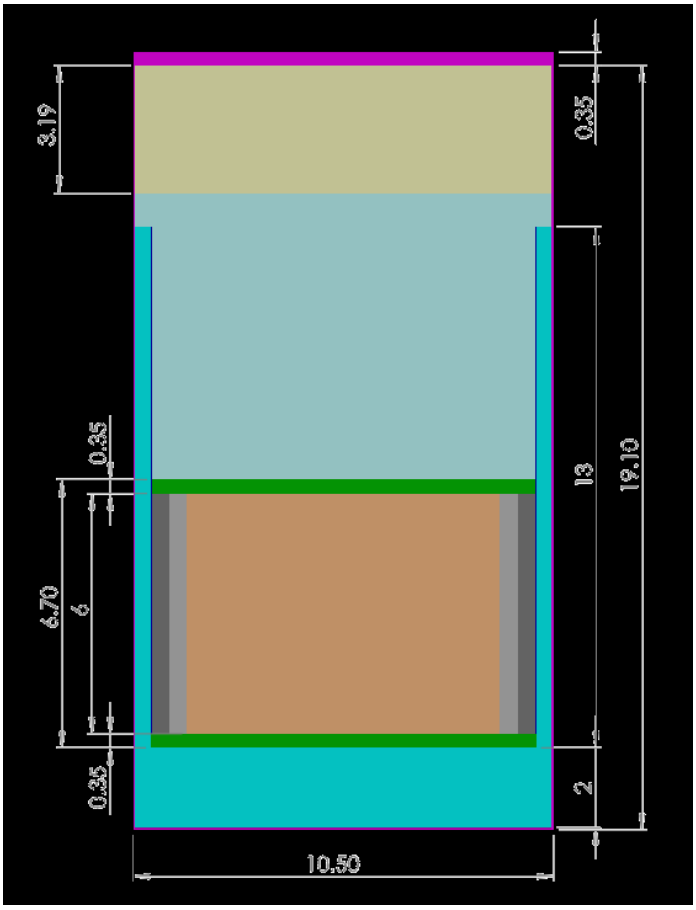

Figure 3-12: AHTR vessel and core major dimensions in meters.

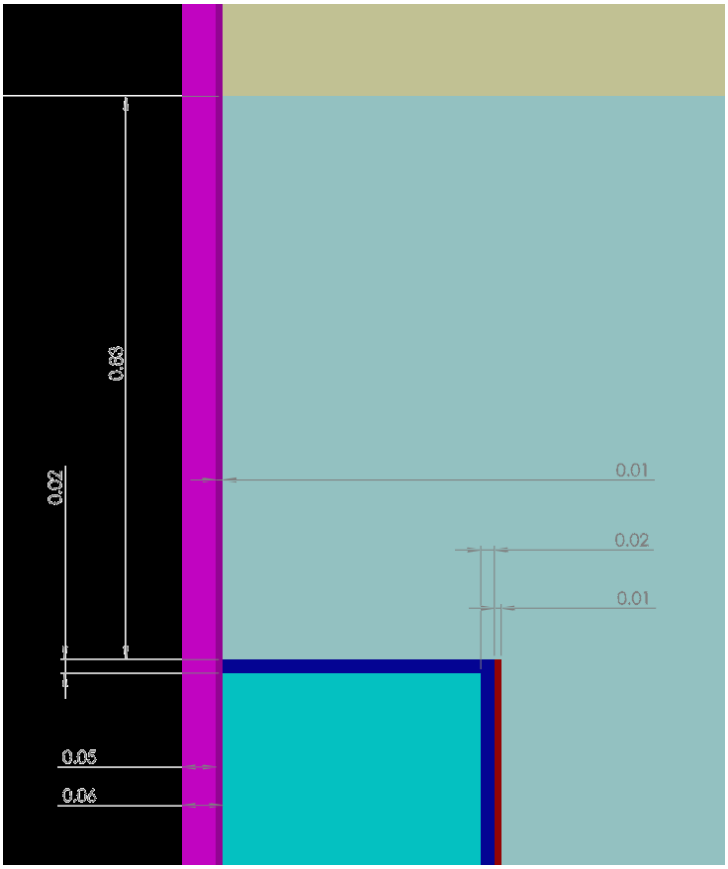

Figure 3-13: Enhanced view of dimensions at the top of the AHTR downcomer.

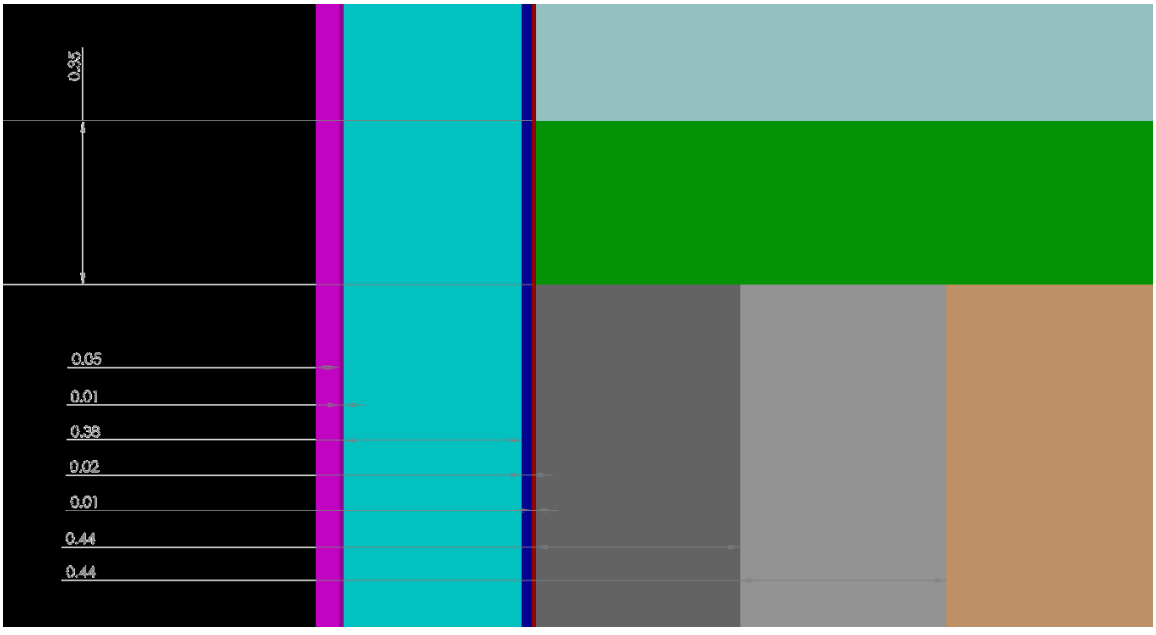

Figure 3-14: Enhanced view of dimensions at the top of the AHTR core.

3.5. Fuel Assembly

Fuel assemblies are made up of 18 fuel plates, grouped in 3 clusters of 6 plates each. Each plate is 2.55 cm thick. The entire fuel assembly is fabricated with **high temperature materials**. The plates in the assembly are 6 m long, the active (fueled) part is 5.5 m (of the total 6 m), and the remaining part (25 cm on top and bottom) are made of reflector material. These plates are enclosed in a **hexagonal C-C** fuel channel box (density 1.95 g/cm^3), which is 1 cm thick. The outer apothem of the box is 22.5 cm, corresponding to 45 cm distance between two parallel outer faces of the box wall. The three symmetric regions (groups of plates) are separated by a Y shaped support structure that is 4 cm thick and made of **C-C composite** (density 1.95 g/cm^3). The coolant channels are 0.7 cm thick, except for the first and last channel of every region, which are half of the full thickness (0.35 cm). Figure 3-15 shows the reference dimensions of the horizontal cross section of the assembly, while Figure 3-16 shows some dimensions that can be derived from the reference dimensions. A three-dimensional view of the fuel assembly structure is given in Figure 3-17.

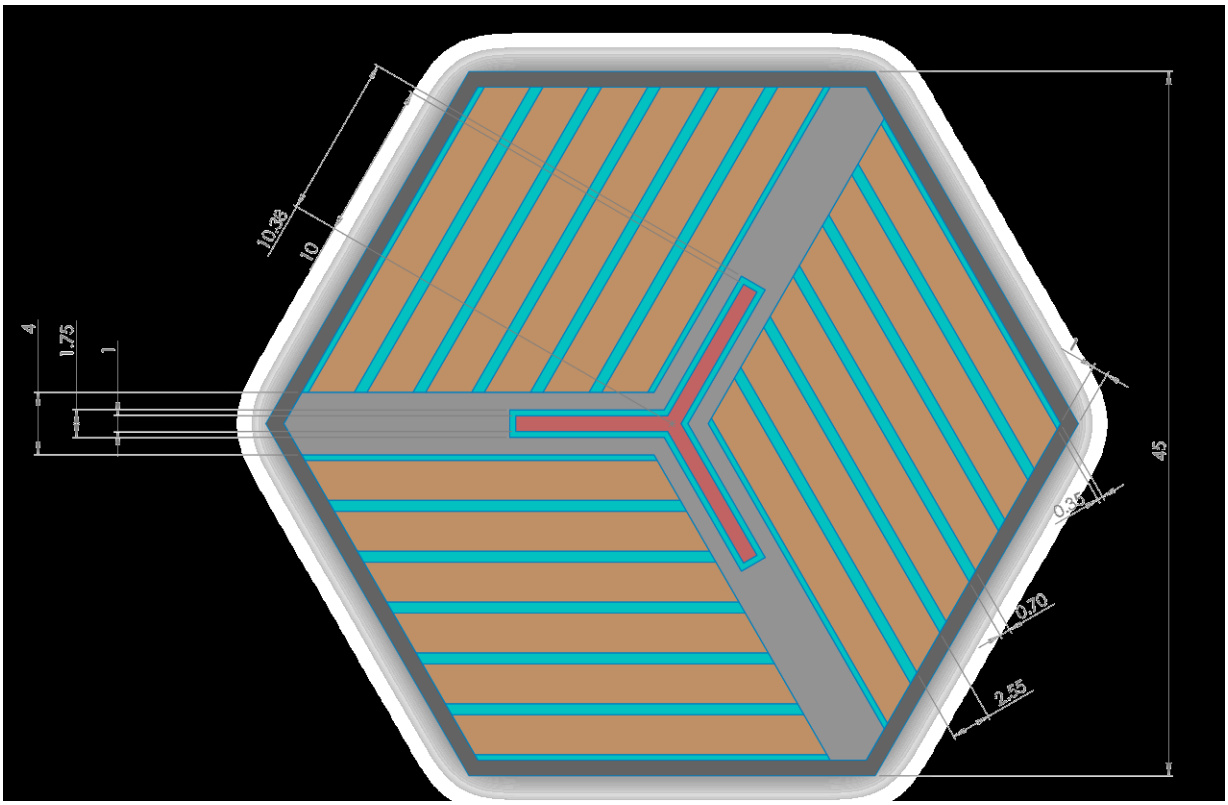

Figure 3-15: AHTR fuel assembly reference dimensions. (Varma, et al., 2012)

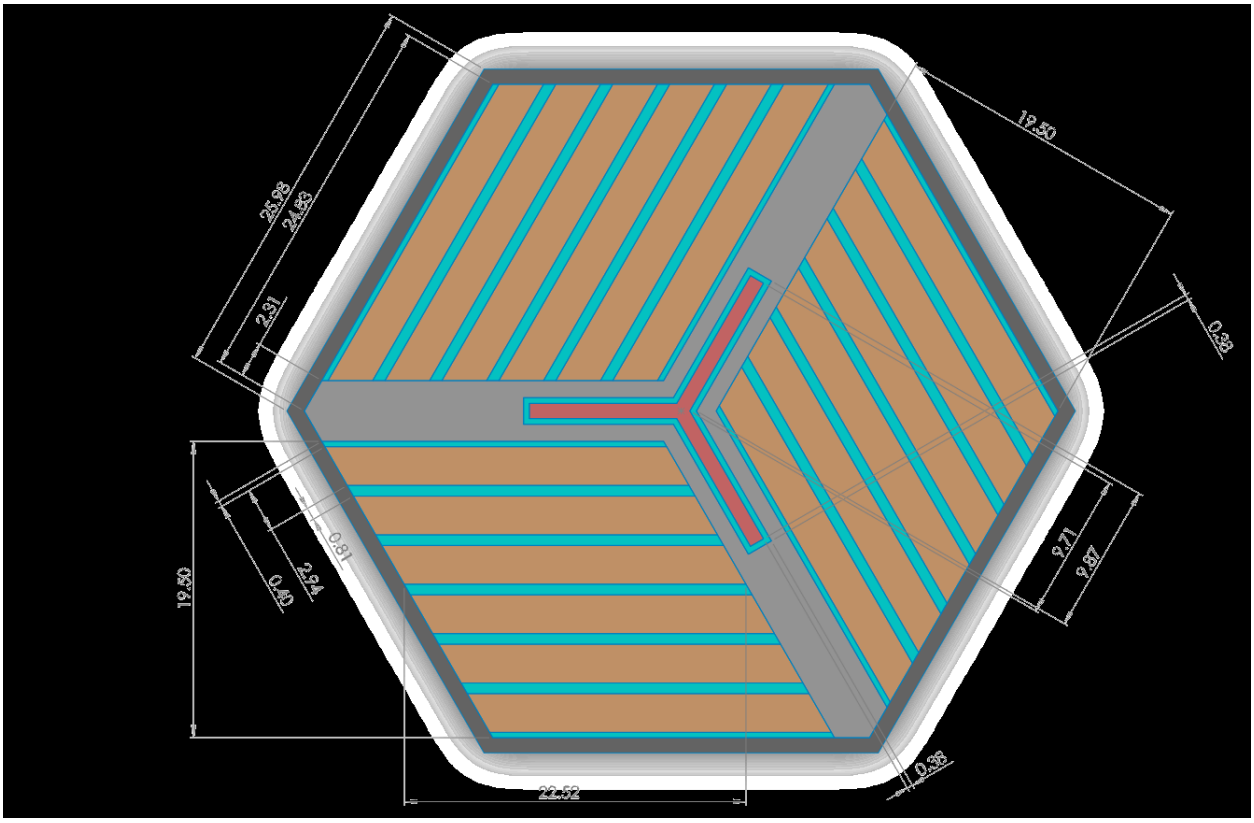

Figure 3-16: AHTR fuel assembly derived dimensions. (Varma, et al., 2012)

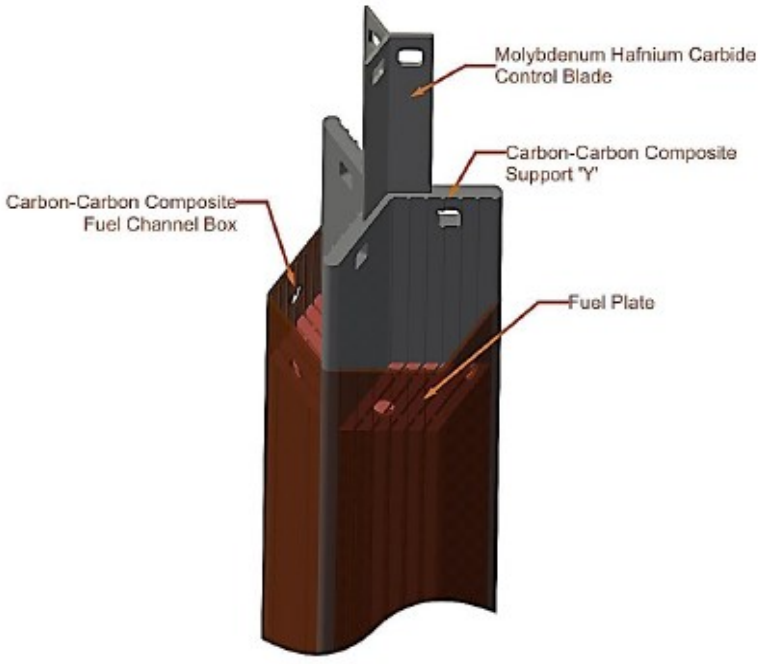

Figure 3-17: AHTR fuel assembly, 3-D view. (Varma, et al., 2012)

The gap between nearby assemblies is 1.8 cm, in order to accommodate for any mechanical distortion. The triangular fuel assembly pitch is then 46.8 cm. Figure 3-18 shows the horizontal cross section of 7 nearby assemblies.

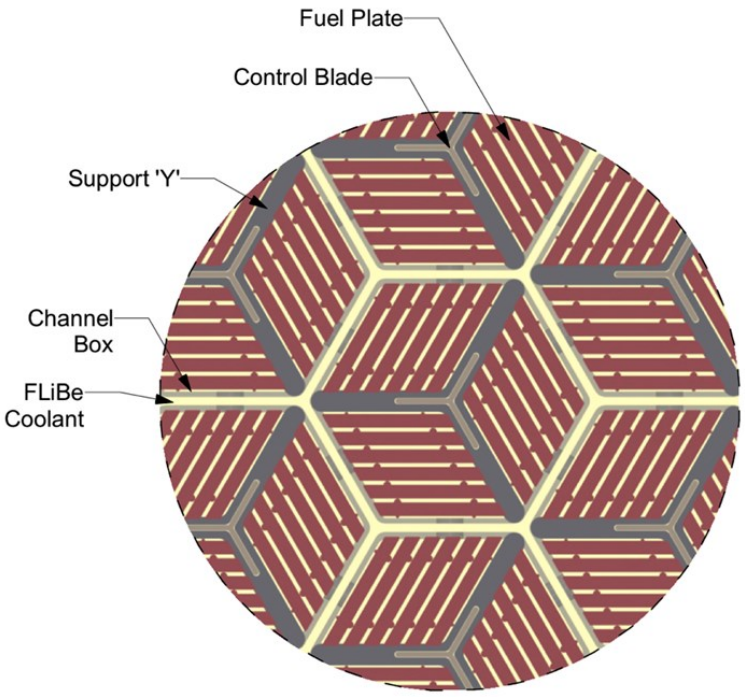

Figure 3-18: Horizontal positioning of the assemblies in the core. (Varma, et al., 2012)

3.5.1. **Control Blade**

Each fuel assembly has its own control blade, with relatively low worth per rod. The Y-shaped control rod is made of **molybdenum hafnium carbide (MHC)** and is inserted into a central Y-shaped support. The MHC is a commercial, particle-strengthened **molybdenum-based alloy with 1.2 wt% Hafnium and 0.1 wt% Carbon**, with a density of 10.28 g/cm^3. The leader rod attaches at the top of the control rod, using the grappling holes, and serves to move the control rod up and down. The Y-shaped control blade slot dimensions are 10.38 cm long for each wing (with respect to the center of the assembly) and 1.75 cm thick. This allows for the Y-shaped control blade to be inserted, which has dimensions of 10 cm long for each wing (with respect to the center of the assembly) and 1 cm thick. Figure 3-19 shows the AHTR control blade geometry.

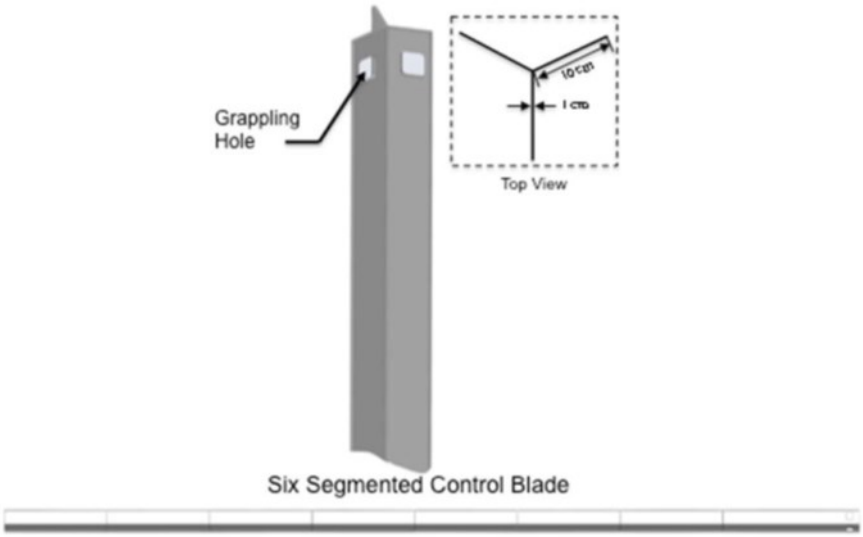

Figure 3-19: AHTR control blade geometry. (Varma, et al., 2012)

3.5.2. **Grappling Collar and Drive Mechanism**

The grappling collar (Figure 3-20) interfaces with upper plate and provides grappling interface for fuel handling.

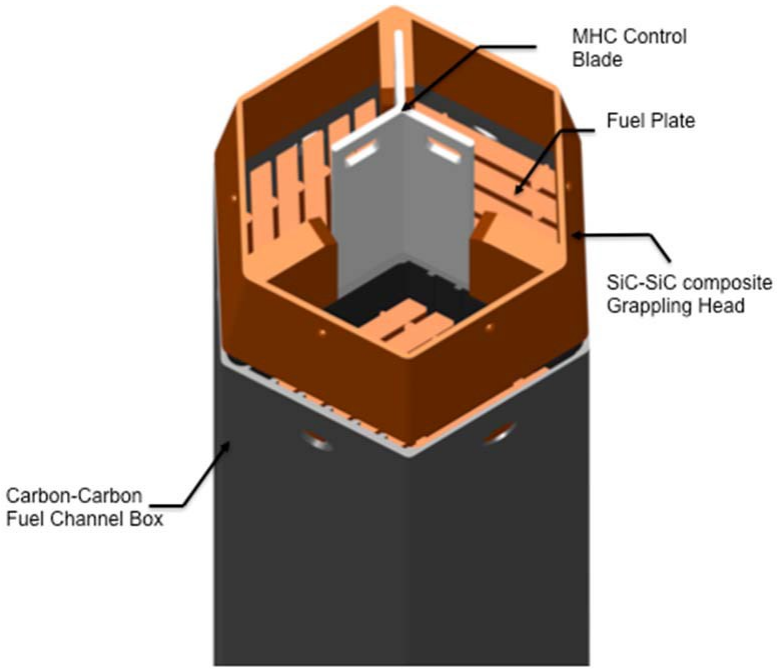

Figure 3-20 AHTR grappling collar in detail. (Varma, et al., 2012)

Each control blade has a leader rod that extends from the top of the control rod to the vessel flange. Each leader rod is encased in a control blade guide tube (Figure 3-21). Leader rod and guide tube are made of **SiC-SiC composite**.

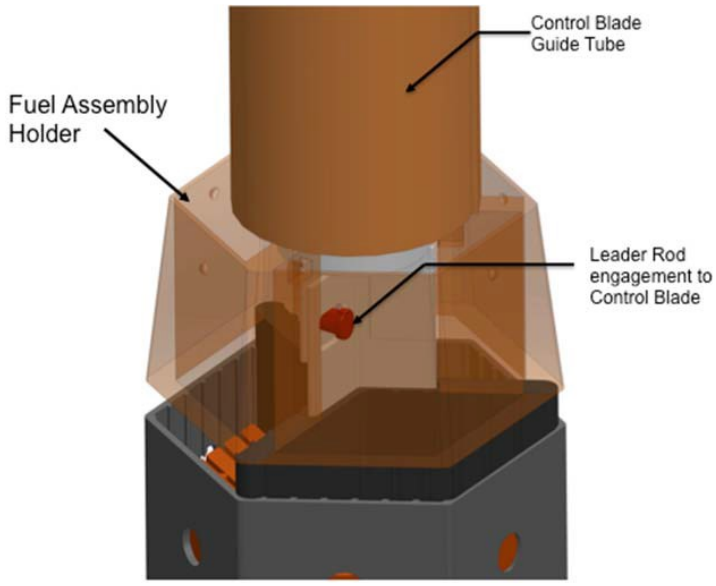

Figure 3-21 Guide tube and grappling collar in detail. (Varma, et al., 2012)

3.6. Fuel Plate

The LSCR fuel plank is shaped as a parallelepiped with two fuel stripes sandwiching a central **carbon slab**. There is a thin 1mm **pyrocarbon** sleeve around the fuel stripes to prevent erosion of TRISO particles. The TRISO fuel particles are randomly dispersed within the fuel strip with a 40% packing fraction in the 2011 model. (Holcomb, et al., 2011) This can be modeled with a TRISO spherical square lattice with a pitch of 0.09265 cm. The newer 2012 reference design has a carbon to heavy metal ratio that is twice as high at 400 compared to the 2011 design. (Varma, et al., 2012) It also has 9 wt% enrichment down from 19.75 wt% enrichment in the preliminary preconceptual design. The enrichment was lowered to reduce the fuel cycle cost and initial capital investment. The 9 wt% enriched fuel has a Carbon to Heavy Metal (CHM) ratio of 400 in the 2012 preconceptual design. The fuel stripe could be made smaller or the packing fraction can be reduced to produce a higher CHM ratio. It is recommended that the fuel stripe thickness be set to contain six fuel layers and a 20% packing fraction. This gives a square pitch of 0.116736 cm. **High density graphite matrix** is inside the fuel stripe in between the TRISO particles. The density of the carbon matrix is 1.75 g/cm^3. Burnable poison particles included near the center of the plate. There are two semi-cylindrical spacers on each of the fuel planks. Figure 3-23 gives a general idea of the configuration of the plate; Figure 3-23 and Figure 3-24 present the dimensions of the plate.

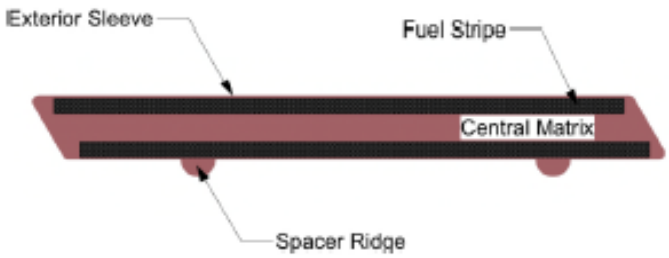

Figure 3-22: Geometrical configuration of the AHTR fuel plate. (Varma, et al., 2012)

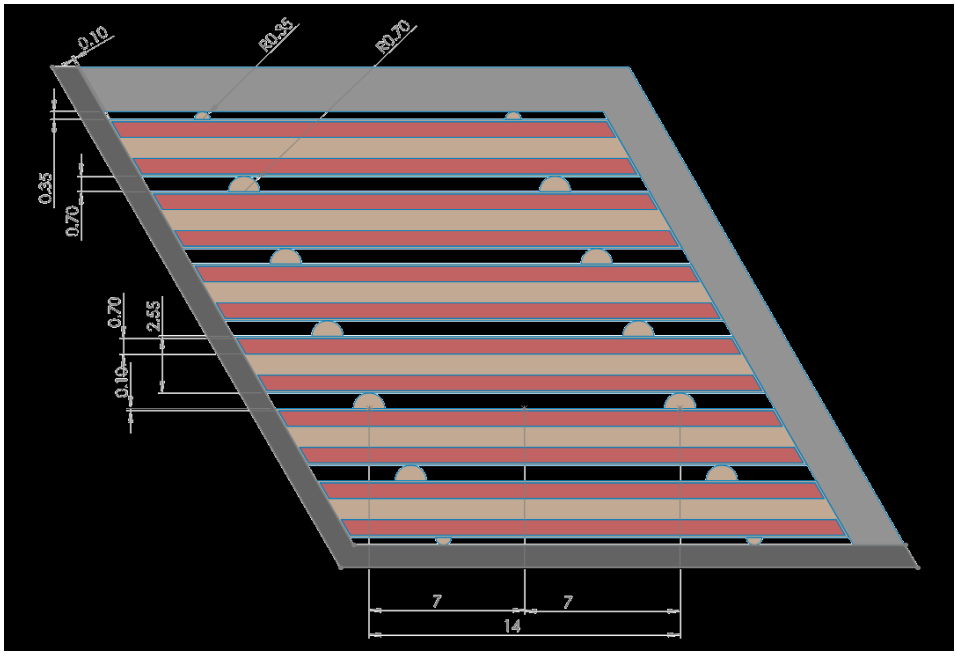

Figure 3-23: Dimensions of the AHTR fuel plate. (Varma, et al., 2012)

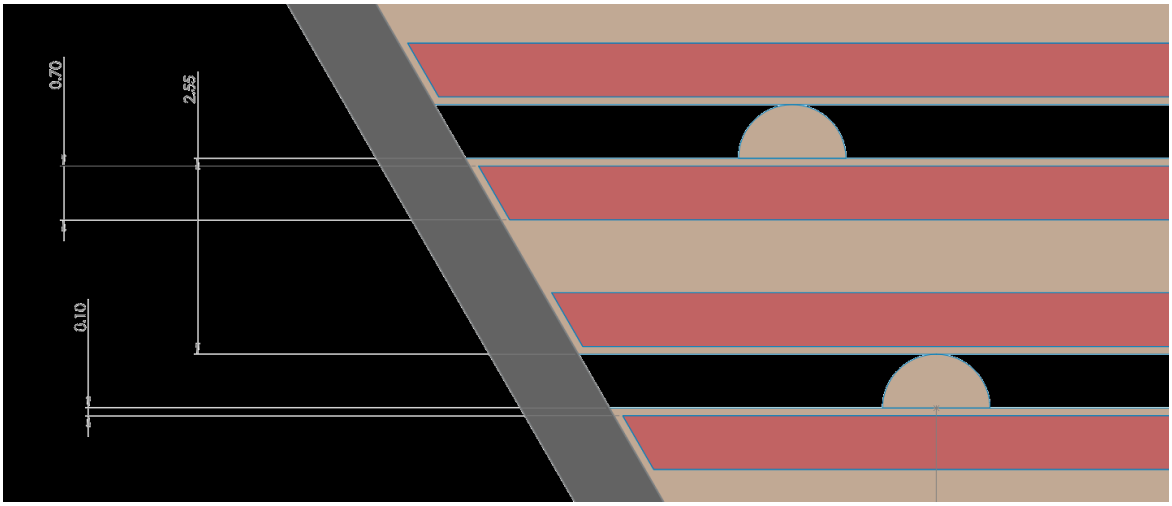

Figure 3-24: Dimensions of the AHTR fuel plate in detail. (Varma, et al., 2012)

3.6.1. **TRISO Particle**

The TRISO fuel particle consists of four layers, an outer **pyrocarbon** layer, **silicon carbide** layer, an inner **pyrocarbon** layer, and a **less dense carbon** buffer layer. Inside of these layers is a **uranium oxycarbide fuel** kernel, Figure 3-25 shows the geometry with the outer layers cut out of the TRISO fuel particle. This fuel is the same as the Advanced Gas Reactor (AGR) fuel developed under DOE-NE sponsorship. The reference irradiation experiment for the fuel type used for the AHTR is AGR-5/6. Fuel enrichment is 9 wt%. Table 3-4 shows the respective dimensions of the TRISO fuel particle.

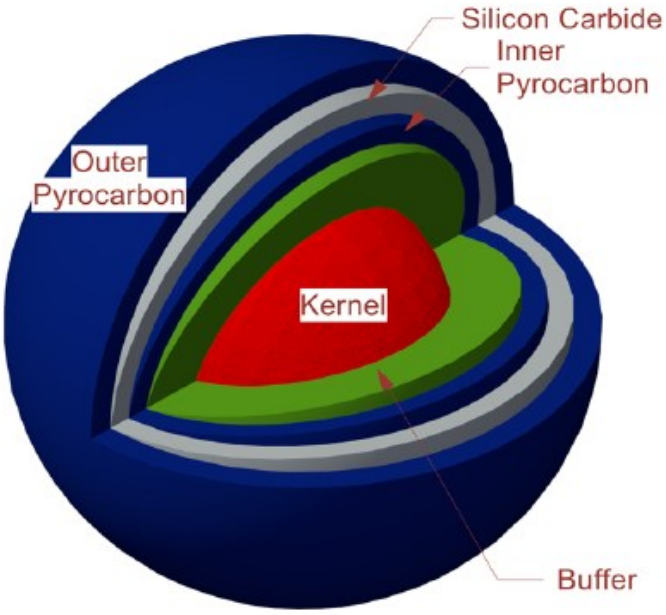

Figure 3-25: TRISO particle geometry configuration. (Varma, et al., 2012)

Table 3-4: TRISO particle parameters.

Region	Parameter	value µm	Material	ρ (g/cm^3)
Kernel	diameter	427	**UCO**	10.9
Buffer	thickness	100	**Porous graphite**	1
IPyC	thickness	35	**Pyrolitic graphite**	1.9
SiC	thickness	35	**SiC**	3.2
OPyC	thickness	40	**Pyrolitic graphite**	1.87
Fuel Particle	diameter	847	----	----

3.6.2. **Burnable Poison**

The burnable poison is located in **Pyrocarbon overcoated sintered grains of Eu_2O_3 powder**; these grains are placed at the center of the plate (Figure 3-26).

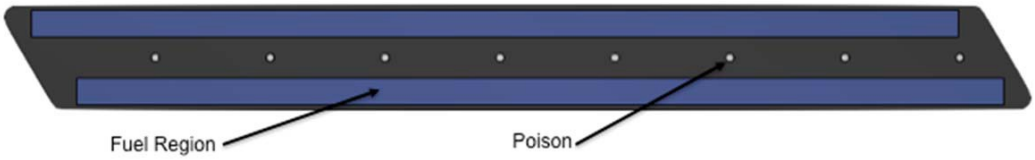

Figure 3-26: Burnable poison grains in the AHTR fuel plate. (Varma, et al., 2012)

Eu_2O_3 has high thermal stability. The melting point is 2,350°C and the density of Eu_2O_3 is 5.0 g/cm^3 (68% of theoretical density). The size and number of Eu_2O_3 grains can be optimized (although, studies available are not very accurate). The final reference design would be 5 grains with radius of 350 micron, In order to provide the required 6 months cycle. (Varma, et al., 2012) For this configuration, the excess reactivity of the core is maintained below 5% for the entire equilibrium cycle.

3.7. Primary Coolant

FLiBe (2LiF-BeF_2) is used as coolant for the primary system and flows over the AHTR core. **Beryllium** provides some moderation, while the **lithium** is ideally isotopically pure ^{7}Li to minimize tritium production. 99.995 wt% ^{7}Li enrichment is generally considered the reference enrichment that can be practically achieved. The salt is transparent and has a density of 1,950 kg/m^3 at 700°C (it is temperature dependent) and a melting point of 459°C. Thus, the salt is in the liquid phase in the primary loop while the reactor is operating, since the core inlet temperature is considered to be 650°C.

3.8. Materials Considered for Different FHR Components

List of different leading materials being considered for the AHTR designs and specific components in these designs have been listed in a recent ORNL report of FHR development roadmap document (Holcomb et al. 2013), and is shown in Table 4.

Table 3-5: Materials Considered for Different FHR Components (Holcomb et al. 2013)

Component or structure	Material *Alternate*
Reactor vessel and primary piping	Alloy 800H with nickel or Alloy N liner *New creep resistant nickel alloy*
Guard vessel	316 stainless steel (SS316)
P-IHX DHX Maintenance heat exchanger	New creep resistant nickel alloy *Alloy N*
Pump (wetted components)	Alloy N *New high-strength nickel alloy*
Core barrel	C-C *SiC/SiC*
Fuel assembly mechanical structure	C-C
Core support plates	SiC/SiC
Ex-core control blade guide	SiC/SiC
Wetted refueling mechanisms	SiC/SiC
Control blades	MHC
Fusible links	Au-Sn alloy
Vessel lid	SS316
Replaceable reflector	Nuclear grade graphite
Permanent reflector	Nuclear grade graphite
Primary salt cleanup reducing agent	Bi-Li alloy
Cleanup system container	C-C *Molybdenum*
High-temperature tritium trap	Yttrium *Samarium*
Intermediate loop piping	Alloy 800H with nickel or Alloy N liner *New creep resistant nickel alloy*
Intermediate to supercritical water heat exchanger	New γ' strengthened nickel alloy *Alloy N*

There are a number of other materials that will be needed for specific components like sensors, valves, or specialized components, that are not listed here. Some of the appropriate materials for those applications are still being developed or optimized while others may be commercially available. PIRT exercise will try to address the availability of appropriate materials for the main components.

4. A Literature Review of Materials Degradation in FHRs

This section provides a brief literature review of materials degradation mechanisms in FHR systems. These mechanisms are caused by the chemical, mechanical, and/or radiation environment. This section highlights some of these challenges and presents a current status report of research in these areas.

4.1. Corrosion Mechanisms

In most high temperature engineering environments, alloys are protected from corrosion with a protective oxide layer which protects the surface from further attack. However, these oxides are readily fluxed (dissolved) by molten salts (Rapp 1987). Furthermore, the lack of oxygen in molten fluoride environment in FHRs prevents regrowth of oxide layers. With the oxides removed, the bare surface of the metals is directly exposed to the environment. In this situation, general corrosion occurs, whereby surface material is oxidized and then dissolved into the surrounding fluid media. In molten fluoride salts (FLiBe and FLiNaK), corrosion rate is determined by redox potential of the molten fluoride coolant, the solubility of corrosion products, transport of oxidizing species to the material surface, and solid state diffusion of active alloying components to the corrosion interface (Olson 2008, Keiser 1977, Sohal 2013).

4.1.1. Thermodynamics of Corrosion Mechanisms

The driving force for thermodynamic dissolution of alloying components is described by the difference in Gibbs free energy between the alloying element and the fluoride salt. Thus for each element, the free energy of fluoride formation per mole is an approximate measure of how readily that element dissociates into the salt. More negative free energies of fluoride formation correspond with increasing stability (Olson 2008). The free energies of salt components are much lower than that of the transition metals commonly used as alloying elements, as shown in Figure 4.1. Chromium forms fluorides more easily than other alloying elements due to its more negative free energy of fluoride formation. Therefore, chromium is expected to be the primary element that dissociates (Richardson 1952). Provided that the molten salt is free from impurities, the driving force for corrosion is small because of the large difference between the free energies of the salt components and the alloying components.

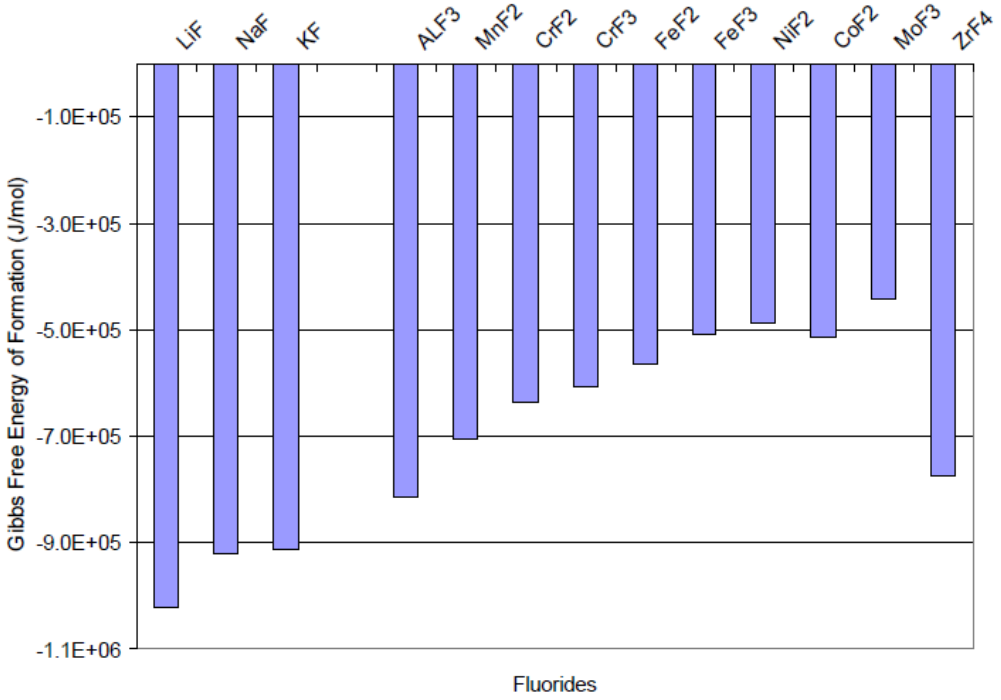

Figure 4-1: Gibbs free energy of fluoride formation for salt components and several common alloying elements at 1027°C (Olson 2008).

4.1.2. **Redox Potential**

The redox potential E of the fluoride salt is a measure of its tendency to undergo oxidation or reduction. It is determined by the equilibrium states of all electrochemical reactions in the salt. It is related to Gibbs free energy change ΔG by

$$\Delta G = -nFE \qquad (1)$$

where n is the number of electrons transferred and F is Faraday's constant.
Redox potential would be an important metric of corrosivity, even if it was difficult to measure. It is easy to measure if there is a stable reference electrode. The redox potential is related to the activities of salt components by the Nernst equation:

$$E = E^0 - \frac{RT}{nF}\ln(Q) \qquad (2)$$

where
E = cell potential at the temperature of interest
E^0 = standard cell potential
R = universal gas constant
T = absolute temperature
n = number of moles of electrons transferred in the cell reaction
F = Faraday constant
Q = reaction quotient, a function of the activities of all chemical species involved in the electrochemical reaction

To measure a redox potential of the salt, one must measure the voltage between an inert electrode and a reference electrode, both electrically connected through the salt. The reference electrode is an electrode which has a stable and well known potential that is independent of changes in the solution of interest. This can be accomplished by using a redox system with each reactant kept at a constant activity. The Ni/Ni^{2+} redox system has been employed successfully for reference electrodes in molten fluorides (Bronstein & Manning 1972). Dynamic reference electrodes have also been demonstrated in FLiBe and FLiNaK (Afonichkin 2009, Durán-Klie 2016).

4.1.3. **Impurity effects**

Impurities in the molten fluoride may increase the redox potential of the salt and can intensify corrosion. These oxidizing impurities include moisture, oxygen, metal oxides, and dissolved polyvalent metal ions. If present in very low quantities, impurity driven corrosion will slow down after the impurities are consumed or when the metal solubility limits of the salt are reached. However, if leaks or other persistent sources of impurities exist, elevated corrosion rates will be sustained until solubility limits are reached (Sohal 2013, Kondo 2009, Ignatiev 2013).

Due to the hygroscopic nature of molten fluorides, moisture impurity is expected at room temperature (Ouyang 2013). However the boiling point of water is 100°C and the decomposition temperatures of hydrated fluorides are even lower, so by the time a fluoride salt reaches its melting temperature above 400°C, almost all the water should evaporate. However, hydrolyzed salts are very difficult to remove from fluoride melts and may not be completely removed during the purification process. The hydrolysis of salt components by water could be a source of HF impurities. As an example, for LiF the reaction is

$$2LiF + H_2O \leftrightarrow Li_2O + 2HF \quad (3)$$

The HF generated in these reactions oxidizes chromium and other alloying elements to form metal fluorides.

$$M^0 + xHF \leftrightarrow \frac{x}{2}H_2 + MF_x \quad (4)$$

Fluorides of nickel and other noble metals can react and oxidize more active metals, particularly chromium.

$$Cr^0 + NiF_2 \leftrightarrow CrF_2 + Ni^0 \quad (5)$$

High valency ions of polyvalent metals, such as Fe^{3+} and Cr^{3+} are soluble in FLiNaK and can oxidize metals (Sohal 2013).

$$2Cr^{3+} + Cr^0 \leftrightarrow 3Cr^{2+} \quad (6)$$

These impurities can be removed from the salt through a number of methods. One method, employed in the MSRE, was to sparge the molten mixture with HF/H_2. The HF reduces oxides and metals in the melt to their respective fluorides, and the H_2 reduces transition metals to their elemental state and physically removes water vapor (Kelleher 2015). The addition of active elements, such as Be or Zr can also be used to control the redox potential by reducing oxidizing impurities (Olson 2008, Sellers 2012). Heating and sparging the salt removes water, though this may risk hydrolysis of the salt[17].

The effect of oxidizing impurities was demonstrated in flow loop corrosion tests at the Kurchatov Institute. When the loop was opened to the air, the redox potential spiked, as shown in Figure 4-2 (Igantiev 2013).

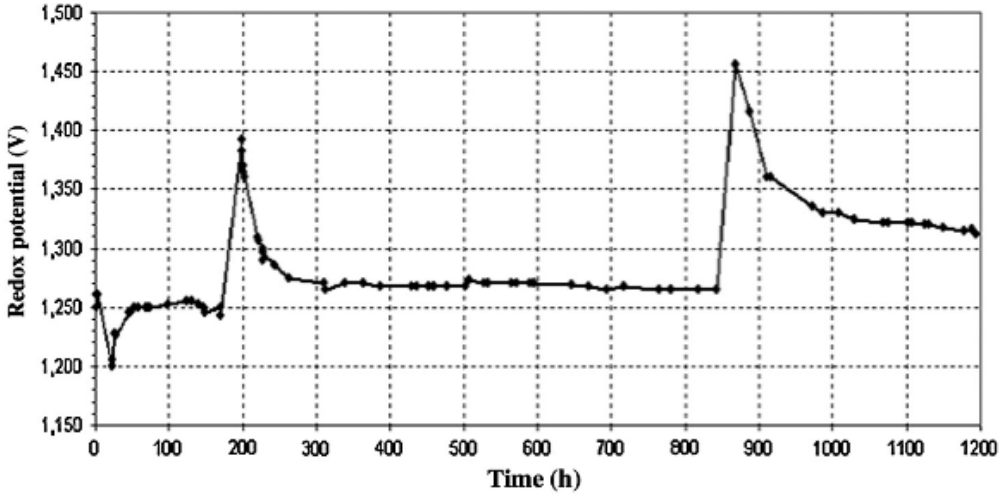

Figure 4-2: Behavior of molten salt redox potential measured relative to dynamic Be reference electrode over time in LiF-NaF-BeF2 corrosion loop. (Ignatiev 2013)

4.1.4. **Galvanic Corrosion or Selective Dissolution**

The ionic nature of molten salts facilitates galvanic corrosion. Galvanic corrosion occurs when two metals with differing electrochemical potentials are in electrical contact and immersed in an electrolyte. A circuit is completed and the metal with a lower electrochemical potential becomes an anode and experience enhanced corrosion while the metal with the higher electrochemical potential becomes the cathode and experiences decreased corrosion. In galvanic corrosion experiments done in FLiNaK shown in Figure 4-3, there is a large galvanic current between the noble metal nickel and the active metal chromium. If dissimilar alloys are used in a reactor, the alloy containing the greatest proportion of chromium and other reactive metals can experience accelerated dissolution (Wang 2014). Galvanic corrosion of this type can be mitigated if a one structural material is used to construct the entire reactor or if the alloys with large difference in their electrochemical potentials are electrically isolated from each other.

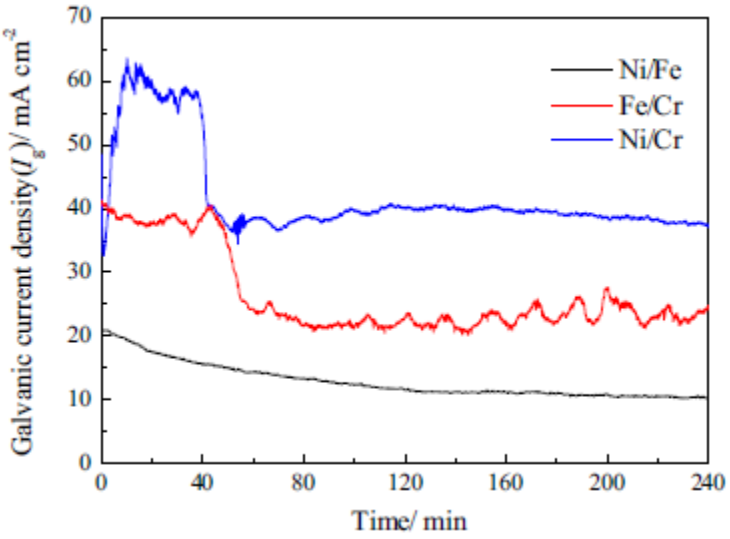

Figure 4-3: The Change in galvanic current density with time for the couples Ni/Fe, Ni/Cr, and Fe/Cr in molten FLiNaK at 700C (Wang 2014)

Galvanic corrosion can also occur on a microscopic scale. On the surface of an alloy, there may exist small spots which are more reactive than the rest of the surface. These spots are some type of defect, often an inclusion, a second phase, or a welded area. These spots become anodic and experience greater selective dissolution than the rest of the surface.

4.1.5. **Temperature-Gradient Driven Corrosion**

Corrosion of transition metals in molten fluoride ceases if the solubility limit of the metal fluoride is reached. But because the solubility of metal fluorides increases with temperature, corrosion can continue if there is temperature gradient in the system. This effect was studied in molten fluoride flow loops during the MSRE. Mass change data over time from one MSRE flow loop is shown in Figure 4-4. Test samples located in the hotter areas of the flow loop lost mass over time, while samples in the cooler areas gained mass (Keiser 1977) .

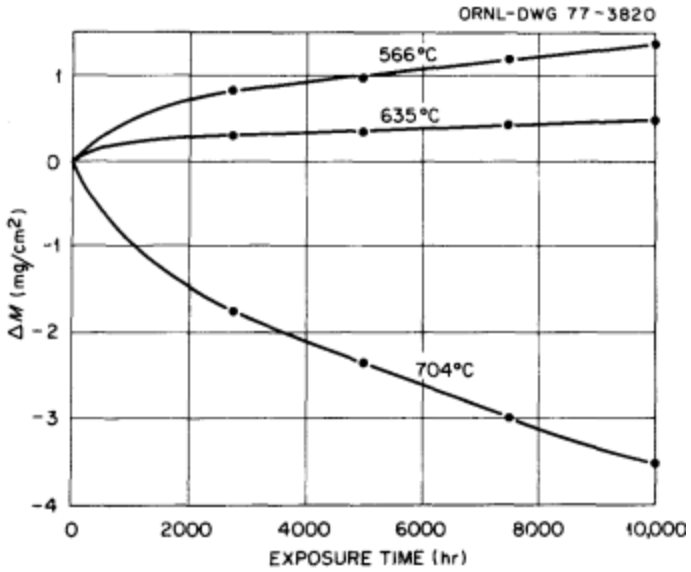

Figure 4-4: Weight change vs exposure time for Hastelloy N speciments exposed to MSBR fuel salt in thermal-convection loop. (Keiser 1977)

4.1.6. **Flow Effects**

The flow conditions in the fluid adjacent to a material's surface can affect the rate of corrosion by increased mass transfer or erosion corrosion. Mass transfer of oxidants from the bulk fluid to the surface increases with increasing fluid velocities and turbulence due to a decrease in boundary layer (diffusion) thickness. The effects of fluid velocity on corrosion rate are illustrated in Figure 4-5. If the corrosion reaction rate is transport limited, the increased fluid velocity will increase corrosion rates. But if the mass transfer rate is faster than the charge transfer rate, the corrosion rate will be activation controlled, and the fluid velocity will have no effect. At high fluid velocities, erosion corrosion can occur. The material surface can be mechanically damaged by shear stress, by impact or abrasion of particles, or by cavitation. If the surface is protected by an oxide layer or a coating, mechanical damage caused by the flowing fluid can expose the underlying material to further attack. However, oxide passive layers are not expected to form or remain on the structural alloys being considered for the FHR structural components.

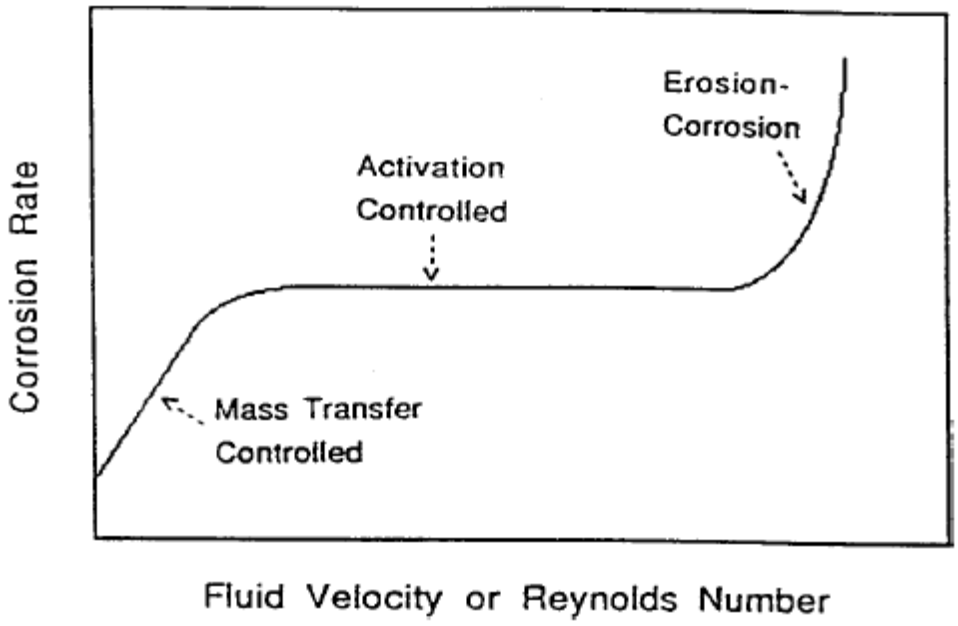

Figure 4-5: Schematic illustration of the variation of corrosion rate with velocity or Reynolds's number (Chen 1992).

4.1.7. **Effect of Alloy Composition and Microstructure**

Alloy composition has a large effect on corrosion rate. Active alloying elements such as chromium and manganese undergo selective dissolution in molten fluorides. Consistently higher corrosion rates have been observed for alloys containing larger percentages of chromium (Sohal 2013). Furthermore, elemental analysis of near-surface regions often shows dealloying of chromium. A schematic of this chromium depletion is shown in Figure 4-6. Near the surface, the chromium concentration is nearly zero. Bulk chromium diffusion is the dominant form of mass transport through grains nearest to the surface. But beyond one grain, chromium diffusion/transportation appears to follow grain boundaries (Zheng 2015).

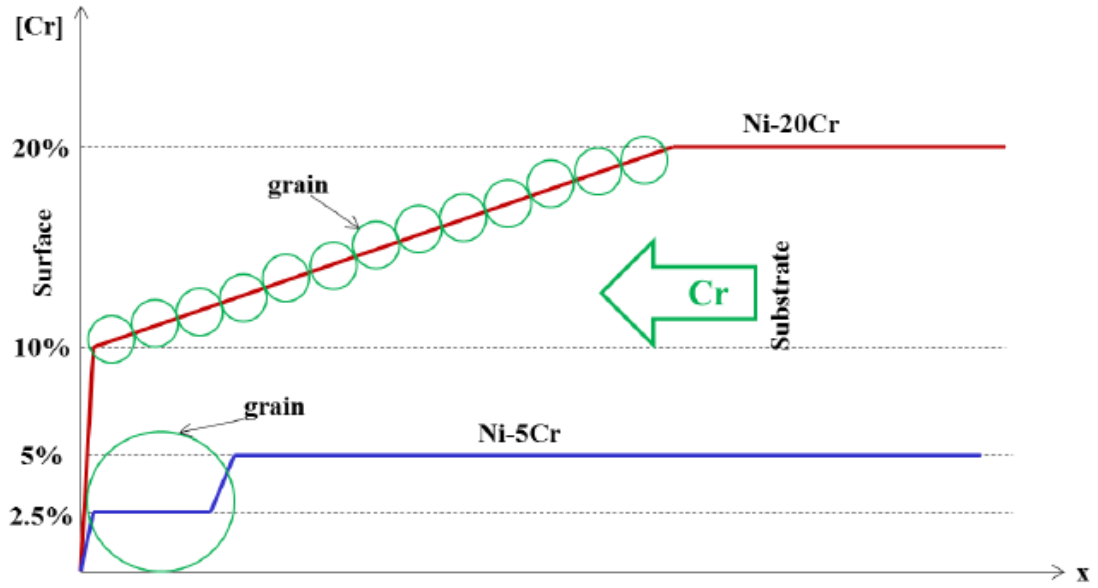

Figure 4-6: Schematic of Cr profile for Ni-20Cr and Ni-5Cr model alloys. (Zheng 2015)

The vacancies left behind chromium dissolution precipitate into voids, and the surface becomes porous. This process is illustrated in Figure 4-7. In Figure 4-8, both voids formation and grain boundary attack can be observed in Incoloy 800-H after 500h exposure to FLiNaK (Olson 2008).

Figure 4-7: Mechanism of subsurface void formation (Richardson 1952).

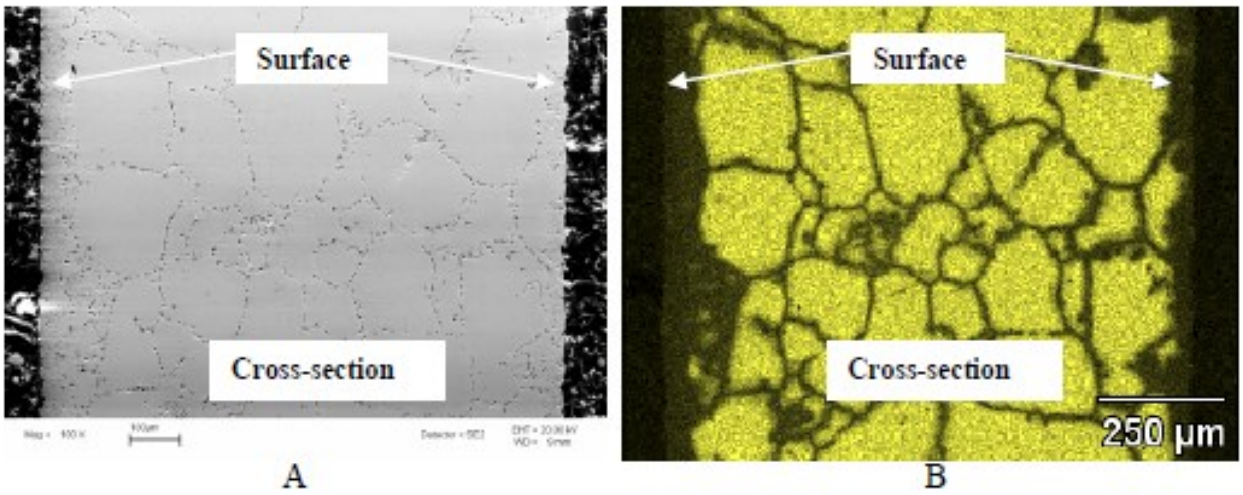

Figure 4-8: A) SEM of Incoloy-800H cross section (~1mm thick) with B) Cr EDS x-ray map. Sample was exposed to FLiNaK at 700C for 500h. (Olson 2008)

4.1.8. **High Temperature Oxidation**

Materials exposed to air during reactor operation must also resist high temperature oxidation. High temperature oxidation resistant alloys typically contain Cr and/or Al which form a protective oxide scale. This scale resists transport of oxygen and moisture to the metallic surface and slows further oxidation. If the protective scale is in any way damaged or unable to form, accelerated corrosion may occur. High temperature oxidation data in air is readily available for all materials under consideration.

4.1.9. **Stress Assisted Corrosion**

Materials under applied mechanical load can experience enhanced corrosion rates. Under certain specific chemical environments and under sustained load causing tensile stresses, crack initiation and growth can be accelerated by the chemical environment. This premature fracture under the combined effect of stress and environment is known as stress corrosion cracking (SCC). Under a cyclic loading conditions, corrosion fatigue (CF) is another failure mechanism, which is less dependent of the specific environments. Stress fluctuations can also be caused by the thermal stresses. However, the overall degradation mode and extent will strongly depend on the environmental parameters as well as cyclic stress parameters like mean stress, stress amplitude, ration of minimum to maximum stress (R-ratio) and frequency. It is not clear if the alloys considered are immune to SCC and CF or not.

4.1.10. **Hydrogen (Tritium) Related Degradation**

Tritium produced in the molten salt as a fission product can potentially participate in degradation mechanisms, depending on the alloys as well as other environmental factors. Different mechanism that are associate with hydrogen are:

- Hydride formation - embrittlement

- Interstitial hydrogen related embrittlement (Solid solution hardening)
- Accumulation of Hydrogen in voids, leading to blistering

4.2. Mechanical/Thermal Degradation Mechanisms

Environmental conditions like temperature as well radiation dose may cause material property variation over time, and possibly lead to material failure. Few possible phenomena are listed here for consideration while selecting appropriate materials for different components of FHR.

4.2.1. **Aging**

Materials held at high temperature for extended periods may experience changes in microstructure. For example, growth of secondary phases can result in precipitation hardening.

4.2.2. **Thermal Cycling**

Temperature variation causes materials to expand and contract due to thermal expansion. This can cause stress in materials if steep temperature gradients are present or if thermal expansion coefficients of different materials are mismatched.

4.2.3. **Creep**

Long term stress below a material's yield stress can cause gradual plastic deformation. Elevated temperatures and high stresses can exacerbate creep.

4.2.4. **Fatigue**

Cyclic loading can cause material damage even when the applied stress is below the yield stress.

4.2.5. **Erosion/Wear**

Materials can experience wear damage if there is side-to-side motion of one solid surface on another. This rubbing can abrade and deform near-surface material.

4.3. Radiation Degradation Mechanisms

4.3.1. **Neutron Activation and Embrittlement**

Neutron flux produced by the chain reaction can generate defects in materials via collision cascades, causing embrittlement. Neutron activation can also degrade materials.

4.3.2. **Radiation Induced Chemical Reactions**

Radiation can induce radiolysis of the molten fluoride, forming corrosive species such as HF. Tritium can also cause (hydrogen) embrittlement of alloys.

5. FHR Materials under Consideration

In a previous publication on FHR roadmap (Holcomb et al. 2013), a list of materials considered for the FHR designs and specific FHR components have been listed. Although new alloys are being optimized and selected for the FHR environments, we have listed the main categories of materials that have been tested or are being considered for different FHR components in different FHR designs.

5.1.1. **Alloys**

5.1.1.1. Structural alloys

Structural alloys in FHRs must have adequate strength at the operating temperature and simultaneously resist corrosion from the contained molten fluoride and resist high temperature oxidation on the air side. A number of Ni-based alloys and stainless steels are being evaluated for FHR structural applications.

5.1.1.1.1. Ni-based alloys

Ni-based alloys have been designed to have high strength and good oxidation resistance at high temperatures. Hastelloy N is a Ni-Mo-Cr alloy which was developed for and used as the primary structural material for the MSRE. It withstood years of operation without incident. Its high Ni content and low Cr content is advantageous in molten fluoride facing materials because it limits the activity of reactive metals which dealloy during exposure. Possible Ni-alloys and their elemental compositions are shown in Table 1.

Table 5-1: Nominal composition of some Ni-based alloys under consideration for FHR applications.

	Ni	Cr	Mo	W	Co	Fe	Mn	Si	Ti	C
Haynes® 230®	bal	22	2	14	<5	<3	<0.5	<0.4	0.3	<0.07
Haynes® 244™	bal	8	22.5	6						<0.01
Hastelloy® N	bal	7	16	<0.5	<0.2	<5	<0.8	<1	<0.35	<.08
Incoloy® 800H	30-35	19-23	<1.5			bal				
Inconel® 600	bal	14-17				6-10	<1	<0.5		<0.05

Improved Ni alloys which are based on Hastelloy N are also being developed. These alloys are designed for increased strength at higher temperatures and improved corrosion resistance.

5.1.1.1.2. Austenitic Stainless Steels

Austenitic stainless steels have good high temperature oxidization resistance at a lower capital cost than Ni-based alloys. However, they have lower corrosion resistance in molten fluoride due because they are Fe based and contain more Cr than Alloy N. Fe far more thermodynamically stable than Cr, but less stable than Ni. Nevertheless, it is believed that corrosion rates of austenitic stainless steels can be managed to acceptable levels by redox control of the salt. Possible grades and their elemental compositions are shown in Table 2.

Table 5-2: Nominal composition of some austenitic stainless steels under consideration for FHR applications.

	Fe	Cr	Mo	Ni	Mn	Ti	Nb	Si	C
SS 304L	bal	18-20		8-10.5	<2			<0.75	<0.08
SS 321	bal	17-19		9-12	<2	<0.7		<1	<0.08
SS 347	bal	17-19		9-12	<2		<1	<0.75	<0.08
SS 316L	bal	16-18	2-3	10-14	<2			<0.75	<0.03

Although austenitic stainless steels 304L and 316L are commonly used alloys in a number of chemical process industry environments, but currently these alloys are not in the ASME nuclear code. However, 304H and 316H with higher carbon content are code qualified. Like other materials that are not in the ASME nuclear code, if 304L and 316L are to be used, they will need to be code qualified.

5.1.1.2. Hardfacing Alloys

Alloys used in pumps and valves require higher high hardness for wear resistance. Possible alloys include Tungsten, TZM and Stellite.

5.1.2. **Carbon containing materials**

Carbon containing materials, such as SiC-SiC composite, CVD SiC, C-C fiber composites, and graphite are being considered for use in reactor core components.
Graphite will be present in large quantities in the reactor core. It can act as a tritium sink. If the graphite is wetted by the fluoride salt, the presence of graphite may increase corrosion of structural alloys by acting as a Cr sink.

5.1.3. **Other materials**

Other materials will be required for special applications, such as sensors. Some examples include optical fiber materials, coatings, and boron nitride. Boron carbide

6. Phenomena Initially Identified for Discussion at PIRT-like Exercise

DISCLAIMER: This section attempts to highlight some of the phenomena initially identified as discussion points for the PIRT-like exercise. This list is in no way a complete description of potential phenomena and may include items which have little or no relevant effects on calculations. These items serve only as a preliminary basis for discussion and will be expanded on by the panel.

- General selection of alloys for different components and possible environment encountered
- Chemical degradation of specific metallic alloys (considered for FHR) in molten FHR salts.
- Possible mechanical property degradation mechanisms
- Microstructural changes due to temperature, environment, and radiation and their effect on corrosion and mechanical properties
- Synergistic effect of environment, mechanical stresses, and radiation on specific degradation mechanisms.

References

[1] V.K. Afonichkin, A.L. Bovet, V. V. Ignatiev, A. V. Panov, V.G. Subbotin, A.I. Surenkov, A.D. Toropov, A.L. Zherebtsov, Dynamic reference electrode for investigation of fluoride melts containing beryllium difluoride, J. Fluor. Chem. 130 (2009) 83–88. doi:10.1016/j.jfluchem.2008.07.017.

[2] H.R. Bronstein, D.L. Manning, Lanthanum Trifluoride as a Membrane in Reference Electrode for Use in Certain Molten Fluorides, J. Electrochem. Soc. 119 (1972) 125–128. doi:10.1149/1.2404146.

[3] T.Y. Chen, A.A. Moccari, D.D. Macdonald, Development of controlled hydrodynamic techniques for corrosion testing, Corrosion. 48 (1992) 239–255. doi:10.5006/1.3315930.

[4] G. Durán-Klie, D. Rodrigues, S. Delpech, Dynamic Reference Electrode development for redox potential measurements in fluoride molten salt at high temperature, Electrochim. Acta. 195 (2016) 19–26. doi:10.1016/j.electacta.2016.02.042.

[5] D.E. Holcomb, G.F. Flanagan, G.T. Mays, W.D. Pointer, K.R. Robb, G.L. Yoder, Fluoride Salt-Cooled High-Temperature Reactor Technology Development and Demonstration Roadmap, Oak Ridge National Laboratory, ORNL/TM-2013/401, 2013.

[6] V. Ignatiev, A. Surenkov, Alloys compatibility in molten salt fluorides: Kurchatov Institute related experience, J. Nucl. Mater. 441 (2013) 592–603. doi:10.1016/j.jnucmat.2013.05.007.

[7] J.R. Keiser, Compatability Studies of Potential Molten-Salt Breeder Reactor Materials in Molten Fluoride Salts, Oak Ridge National Laboratory, ORNL-TM-5783, 1977.

[8] B.C. Kelleher, Purification and Chemical Control of Molten Li2BeF4 for a Fluoride Salt Cooled Reactor, PhD thesis, University of Wisconsin at Madison, 2015.

[9] M. Kondo, T. Nagasaka, T. Muroga, A. Sagara, N. Noda, Q. Xu, D. Ninomiya, N. Masaru, A. Suzuki, T. Terai, High performance corrosion resistance of nickel-based alloys in molten salt flibe, Fusion Sci. Technol. 56 (2009) 190–194.

[10] L.C. Olson, J.W. Ambrosek, K. Sridharan, M.H. Anderson, T.R. Allen, Materials corrosion in molten LiF-NaF-KF salt, J. Fluor. Chem. (2009). doi:10.1016/j.jfluchem.2008.05.008.

[11] F.Y. Ouyang, C.H. Chang, B.C. You, T.K. Yeh, J.J. Kai, Effect of moisture on corrosion of Ni-based alloys in molten alkali fluoride FLiNaK salt environments, J. Nucl. Mater. 437 (2013) 201–207. doi:10.1016/j.jnucmat.2013.02.021.

[12] F. Rahnema, B. Petrovic, C. Edgar, D. Zhang, P. Avigni, M. Huang, S. Terlizzi, The Currrent Status of the Tools for Modeling and Simulation of Advanced High Temperature

Reactor Neutronics Analysis, Whitepaper for neutronics PIRT, CRMP-2015-12-001, 2015.

[13] R.A. Rapp, Chemistry and electrochemistry of hot corrosion of metals, Mater. Sci. Eng. 87 (1987) 319–327. doi:10.1016/0025-5416(87)90394-6.

[14] L.S. Richardson, D.C. Vreeland, W.D. Manly, Corrosion by Molten Fluorides, Oak Ridge National Laboratory, ORNL 1491, 1952.

[15] M.S. Sohal, M.A. Ebner, P. Sabharwall, P. Sharpe, Engineering Database of Liquid Salt Thermophysical and Thermochemical Properties, Idaho National Laboratory, 2013. INL/EXT-10-18297

[16] Y. Wang, H. Liu, C. Zeng, Galvanic corrosion of pure metals in molten fluorides, J. Fluor. Chem. 165 (2014) 1–6. doi:10.1016/j.jfluchem.2014.05.010.

[17] G. Zheng, Corrosion Behavior of Alloys in Molten Fluoride Salts, PhD thesis, University of Wisconsin at Madison, 2015.

7. Appendix

7.1. Supplementary References:

[1] V. Bernardet, S. Gomes, S. Delpeux, M. Dubois, K. Guérin, D. Avignant, G. Renaudin, L. Duclaux, Protection of nuclear graphite toward fluoride molten salt by glassy carbon deposit, J. Nucl. Mater. 384 (2009) 292–302. doi:10.1016/j.jnucmat.2008.11.032.

[2] W.-J. Cheng, R.S. Sellers, M.H. Anderson, K. Sridharan, C.-J. Wang, T.R. Allen, Zirconium effect on the corrosion behavior of 316L stainless steel alloy and Hastelloy-N superalloy in molten fluoride salt, Nucl. Technol. 183 (2013) 248–259. doi:10.13182/NT12-125.

[3] V. Danielik, P. Fellner, O. Matal, Corrosion of Nickel in the Molten Mixture LiF-NaF-ZrF 4, Acta Chim. Slovaca. 2 (2009) 3–11.

[4] S. Delpech, C. Cabet, C. Slim, G.S. Picard, Molten fluorides for nuclear applications, Mater. Today. 13 (2010) 34–41. doi:10.1016/S1369-7021(10)70222-4.

[5] B. El-Dasher, J. Farmer, J. Ferreira, M.S. de Caro, A. Rubenchik, A. Kimura, Corrosion of oxide dispersion strengthened iron–chromium steels and tantalum in fluoride salt coolant: An in situ compatibility study for fusion and fusion–fission hybrid reactor concepts, J. Nucl. Mater. 419 (2011) 15–23. doi:10.1016/j.jnucmat.2011.07.036.

[6] S. Fabre, C. Cabet, L. Cassayre, P. Chamelot, S. Delepech, J. Finne, L. Massot, D. Noel, Use of electrochemical techniques to study the corrosion of metals in model fluoride melts, J. Nucl. Mater. 441 (2013) 583–591. doi:10.1016/j.jnucmat.2013.03.055.

[7] M. Gibilaro, L. Massot, P. Chamelot, A way to limit the corrosion in the Molten Salt Reactor concept: the salt redox potential control, Electrochim. Acta. 160 (2015) 209–213. doi:10.1016/j.electacta.2015.01.142.

[8] X. He, J. Song, J. Tan, B. Zhang, H. Xia, Z. He, X. Zhou, M. Zhao, X. Liu, L. Xu, S. Bai, SiC coating: An alternative for the protection of nuclear graphite from liquid fluoride salt, J. Nucl. Mater. 448 (2014) 1–3. doi:10.1016/j.jnucmat.2014.01.034.

[9] Z. He, L. Gao, X. Wang, B. Zhang, W. Qi, J. Song, X. He, C. Zhang, H. Tang, H. Xia, X. Zhou, Improvement of stacking order in graphite by molten fluoride salt infiltration, Carbon N. Y. 72 (2014) 304–311. doi:10.1016/j.carbon.2014.02.010.

[10] D.E. Holcomb, G.F. Flanagan, G.T. Mays, W.D. Pointer, K.R. Robb, G.L. Yoder, Fluoride Salt-Cooled High-Temperature Reactor Technology Development and Demonstration Roadmap, Oak Ridge National Laboratory, ORNL/TM-2013/401, 2013.

[11] V. Ignatiev, A. Surenkov, Corrosion phenomena induced by molten salts in Generation IV nuclear reactors, in: Pascal Yvon (Ed.), Struct. Mater. Gener. IV Nucl. React., Elsevier Science & Technology, 2016: pp. 153–189. doi:10.1016/B978-0-08-100906-2.00005-7.

[12] V. Ignatiev, A. Surenkov, Alloys compatibility in molten salt fluorides: Kurchatov Institute related experience, J. Nucl. Mater. (2013). doi:10.1016/j.jnucmat.2013.05.007.

[13] B.C. Kelleher, Purification and Chemical Control of Molten Li2BeF4 for a Fluoride Salt Cooled Reactor, PhD thesis, University of Wisconsin at Madison, 2015.

[14] J.W. Koger, Fluoride Salt Corrosion and Mass Transfer in High Temperature Dynamic Systems, CORROSION. 29 (1973) 115–122. doi:10.5006/0010-9312-29.3.115.

[15] J.W. Koger, Corrosion Product Deposition in Molten Fluoride Salt Systems, CORROSION. 30 (1974) 125–130. doi:10.5006/0010-9312-30.4.125.

[16] M. Kondo, T. Nagasaka, T. Muroga, A. Sagara, N. Noda, Q. Xu, D. Ninomiya, N. Masaru, A. Suzuki, T. Terai, High performance corrosion resistance of nickel-based alloys in molten salt flibe, Fusion Sci. Technol. 56 (2009) 190–194.

[17] M. Kondo, T. Nagasaka, A. Sagara, N. Noda, T. Muroga, Q. Xu, M. Nagura, A. Suzuki, T. Terai, Metallurgical study on corrosion of austenitic steels in molten salt LiF-BeF2 (Flibe), J. Nucl. Mater. 386–388 (2009) 685–688. doi:10.1016/j.jnucmat.2008.12.317.

[18] M. Kondo, T. Nagasaka, V. Tsisar, A. Sagara, T. Muroga, T. Watanabe, T. Oshima, Y. Yokoyama, H. Miyamoto, E. Nakamura, N. Fujii, Corrosion of Reduced Activation

Ferritic Martensitic steel JLF-1 in purified Flinak at static and flowing conditions, Fusion Eng. Des. 85 (2010) 1430–1436. doi:10.1016/j.fusengdes.2010.03.064.

[19] M. Kondo, T. Nagasaka, Q. Xu, T. Muroga, A. Sagara, N. Noda, D. Ninomiya, M. Nagura, A. Suzuki, T. Terai, N. Fujii, Corrosion characteristics of reduced activation ferritic steel, JLF-1 (8.92Cr-2W) in molten salts Flibe and Flinak, Fusion Eng. Des. 84 (2009) 1081–1085. doi:10.1016/j.fusengdes.2009.02.046.

[20] L. Král, J. Čermák, O. Matal, T. Šimo, L. Nesvadba, Corrosion of chosen Ni-based material exposed to LiF-NaF molten salts, in: Met. 2010 19th Int. Conf. Metall. Mater., 2010: pp. 596–600.

[21] X.L. Li, S.M. He, X.T. Zhou, P. Huai, Z.J. Li, A.G. Li, X.H. Yu, High-temperature corrosion behavior of Ni-16Mo-7Cr-4Fe superalloy containing yttrium in molten LiF-NaF-KF salt, J. Nucl. Mater. 464 (2015) 342–345. doi:10.1016/j.jnucmat.2015.05.007.

[22] M. Liu, J. Zheng, Y. Lu, Z. Li, Y. Zou, X. Yu, X. Zhou, Investigation on corrosion behavior of Ni-based alloys in molten fluoride salt using synchrotron radiation techniques, J. Nucl. Mater. 440 (2013) 124–128. doi:10.1016/j.jnucmat.2013.04.056.

[23] H.E. McCoy, R.L. Beatty, W.H. Cook, R.E. Gehlbach, C.R. Kennedy, J.W. Koger, A.P. Litman, C.E. Sessions, J.R. Weir, NEW DEVELOPMENTS IN MATERIALS FOR MOLTEN-SALT REACTORS, Nucl. Appl. Technol. 8 (1970) 156–169.

[24] L.C. Olson, Materials Corrosion in Molten LiF-NaF-KF Eutectic Salt, PhD thesis, University of Wisconsin at Madison, 2009.

[25] L.C. Olson, J.W. Ambrosek, K. Sridharan, M.H. Anderson, T.R. Allen, Materials corrosion in molten LiF-NaF-KF salt, J. Fluor. Chem. 130 (2009) 67–73. doi:10.1016/j.jfluchem.2008.05.008.

[26] F.Y. Ouyang, C.H. Chang, J.J. Kai, Long-term corrosion behaviors of Hastelloy-N and Hastelloy-B3 in moisture-containing molten FLiNaK salt environments, J. Nucl. Mater. 446 (2014) 81–89. doi:10.1016/j.jnucmat.2013.11.045.

[27] F.Y. Ouyang, C.H. Chang, B.C. You, T.K. Yeh, J.J. Kai, Effect of moisture on corrosion of Ni-based alloys in molten alkali fluoride FLiNaK salt environments, J. Nucl. Mater. 437 (2013) 201–207. doi:10.1016/j.jnucmat.2013.02.021.

[28] J. Qiu, Y. Zou, G. Yu, H. Liu, Y. Jia, Z. Li, P. Huai, X. Zhou, H. Xu, Compatibility of container materials with Cr in molten FLiNaK salt, J. Fluor. Chem. 168 (2014) 69–74. doi:10.1016/j.jfluchem.2014.09.010.

[29] R.S. Sellers, W. Cheng, M.H. Anderson, K. Sridharan, C. Wang, T.R. Allen, Materials Corrosion in Molten LiF-NaF-KF Eutectic Salt Under Different Reduction-Oxidation

Conditions, in: Int. Congr. Adv. Nucl. Power Plants 2012, ICAPP 2012, June 24, 2012 - June 28, 2012: pp. 953–961.

[30] J. Serp, M. Allibert, O. Beneš, S. Delpech, O. Feynberg, V. Ghetta, D. Heuer, D. Holcomb, V. Ignatiev, J.L. Kloosterman, L. Luzzi, E. Merle-Lucotte, J. Uhlíř, R. Yoshioka, D. Zhimin, The molten salt reactor (MSR) in generation IV: Overview and perspectives, Prog. Nucl. Energy. 77 (2014) 308–319. doi:10.1016/j.pnucene.2014.02.014.

[31] S.L. Shrestha, D. Bhattacharyya, G. Yuan, Z.J. Li, E. Budzakoska-Testone, M. De Los Reyes, M. Drew, L. Edwards, Creep resistance and material degradation of a candidate Ni–Mo–Cr corrosion resistant alloy, Mater. Sci. Eng. A. 674 (2016) 64–75. doi:10.1016/j.msea.2016.07.032.

[32] M.S. Sohal, M.A. Ebner, P. Sabharwall, P. Sharpe, Engineering Database of Liquid Salt Thermophysical and Thermochemical Properties, Idaho National Laboratory, INL/EXT-10-18297, 2013.

[33] Y.L. Wang, Q. Wang, H.J. Liu, C.L. Zeng, The effect of the microstructure on the corrosion behavior of N5 superalloy in a molten (Li,Na,K)F eutectic salt, RSC Adv. 5 (2015) 32755–32760. doi:10.1039/C5RA04755B.

[34] Y.L. Wang, Q. Wang, H.J. Liu, C.L. Zeng, Effect of grain refinement on the corrosion of Ni-Cr alloys in molten (Li,Na,K)F, Corros. Sci. 109 (2016) 43–49. doi:10.1016/j.corsci.2016.03.027.

[35] Y.L. Wang, Q. Wang, H.J. Liu, C.L. Zeng, Effects of the oxidants H2O and CrF3 on the corrosion of pure metals in molten (Li,Na,K)F, Corros. Sci. 103 (2016) 268–282. doi:10.1016/j.corsci.2015.11.032.

[36] Y. Wang, Z.-F. Tang, Y. Fu, S.-R. Huang, S.-F. Zhao, P. Zhang, L.-D. Xie, X.-G. Wang, G.-J. Zhang, Corrosion behavior of ZrC–SiC composite ceramics in LiF–NaF–KF molten salt at high temperatures, Ceram. Int. 41 (2015) 12996–13005. doi:10.1016/j.ceramint.2015.06.143.

[37] Y. Wang, H. Liu, G. Yu, J. Hou, C. Zeng, Electrochemical study of the corrosion of a Ni-based alloy GH3535 in molten (Li,Na,K)F at 700 8C, J. Fluor. Chem. 178 (2015) 14–22. doi:10.1016/j.jfluchem.2015.06.014.

[38] Y. Wang, H. Liu, C. Zeng, Galvanic corrosion of pure metals in molten fluorides, J. Fluor. Chem. 165 (2014) 1–6. doi:10.1016/j.jfluchem.2014.05.010.

[39] D.F. Williams, L.M. Toth, K.. Clarno, Assessment of Candidate Molten Salt Coolants for the NGNP/NHI Heat-Transfer Loop, Oak Ridge National Laboratory, ORNL/TM-2006/69, 2006.

[40] D.F. Wilson, Chemical compatibility issues associated with use of SiC/SiC in advanced reactor concepts, Oak Ridge National Laboratory, ORNL/TM-2013/401, 2012.

[41] W. Xue, X. Yang, J. Qiu, H. Liu, B. Zhao, H. Xia, X. Zhou, P. Huai, H. Liu, J. Wang, Effects of Cr3+ on the corrosion of SiC in LiF–NaF–KF molten salt, Corros. Sci. 114 (2017) 96–101. doi:10.1016/j.corsci.2016.10.026.

[42] X. Yang, S. Feng, X. Zhou, H. Xu, T.K. Sham, Interaction between nuclear graphite and molten fluoride salts: A synchrotron radiation study of the substitution of graphitic hydrogen by fluoride ion, J. Phys. Chem. A. (2012). doi:10.1021/jp208990y.

[43] X. Yang, M. Liu, Y. Gao, D. Zhang, S. Feng, H. Liu, G. Yu, G. Wu, M. Wang, X. Zhou, H. Xia, P. Huai, T.K. Sham, J. Wang, J. Guo, Effect of oxygen on the corrosion of SiC in LiF–NaF–KF molten salt, Corros. Sci. 103 (2016) 165–172. doi:10.1016/j.corsci.2015.11.014.

[44] X. Yang, D. Zhang, M. Liu, S. Feng, W. Xue, H. Liu, G. Yu, X. Zhou, H. Xia, P. Huai, Z. Li, Y. Lu, H. Zhou, S. Dong, Corrosion of SiC induced by Hastelloy N alloy and its corrosion products in LiF–NaF–KF molten salt, Corros. Sci. 109 (2016) 62–67. doi:10.1016/j.corsci.2016.03.029.

[45] X.-X. Ye, H. Ai, Z. Guo, H. Huang, L. Jiang, J. Wang, Z. Li, X. Zhou, The high-temperature corrosion of Hastelloy N alloy (UNS N10003) in molten fluoride salts analysed by STXM, XAS, XRD, SEM, EPMA, TEM/EDS, Corros. Sci. 106 (2016) 249–259. doi:10.1016/j.corsci.2016.02.010.

[46] G. Zheng, Corrosion Behavior of Alloys in Molten Fluoride Salts, PhD thesis, University of Wisconsin at Madison, 2015.

[47] G. Zheng, B. Kelleher, G. Cao, M. Anderson, T. Allen, K. Sridharan, Corrosion of 316 stainless steel in high temperature molten Li2BeF4 (FLiBe) salt, J. Nucl. Mater. 461 (2015) 143–150. doi:10.1016/j.jnucmat.2015.03.004.

[48] Y. Zhu, J. Hou, G. Yu, J. Qiu, S. Chen, X. Zhou, Effects of exposing temperature on corrosion performance of weld joint of a Ni–Mo–Cr alloy, J. Fluor. Chem. 182 (2016) 69–75. doi:10.1016/j.jfluchem.2015.12.005.

7.2. ORNL Reports Related to MSR Materials

[1] G.M. Adamson, R.S. Crouse, W.D. Manly, Interim Report on Corrosion by Alkali-Metal Fluorides: Work to May 1, 1953, Oak Ridge National Laboratory, ORNL-2337, 1959.

[2] G.M. Adamson, R.S. Crouse, W.D. Manly, Interim Report on Corrosion by Zirconium-Base Fluorides, Oak Ridge National Laboratory, ORNL-2338, 1961.

[3] J.H. DeVan, Effect of Alloying Additions on Corrosion Behavior of Nickel - Molybdenum Alloys in Fused Fluoride Mixtures, Oak Ridge National Laboratory, ORNL-TM-2021, 1967.

[4] J.H. DeVan, R.B.I. Evans, Corrosion Behavior of Reactor Materials in Fluoride Salt Mixtures, Oak Ridge National Laboratory, ORNL/TM-0328, 1962.

[5] R.B. Evan, J.W. Koger, J.H. DeVan, Corrosion in Polythermal Loop Systems II. A Solid-State Diffusion Mechanism with and without Liquid Film Effects, Oak Ridge National Laboratory, ORNL-4575, 1971.

[6] R.B.I. Evans, J.H. DeVan, G.M. Watson, Self-Diffusion of Chromium in Nickel-Base Alloys, Oak Ridge National Laboratory, ORNL-2982, 1961.

[7] W.R. Grimes, Chemical Research and Development for Molten-Salt Breeder Reactors, Oak Ridge National Laboratory, ORNL/TM-1853, 1967.

[8] D.G. Harman, Postirradiation Tensile and Creep-Rupture Properties of Several Experimental Heats of Incoloy 800 at 700 and 760 C, Oak Ridge National Laboratory, ORNL/TM-2305, 1968.

[9] P.R. Kasten, E.S. Bettis, W.H. Cook, W.P. Eatherly, D.K. Holmes, R.J. Kedl, C.R. Kennedy, S.S. Krislis, H.E. McCoy, A.M. Perry, R.C. Robertson, D. Scott, R.A. Strehlow, Graphite Behavior and its Effects on MSBR Performance, Oak Ridge National Laboratory, Oak Ridge National Laboratory, ORNL/TM-2136, 1969.

[10] G.W. Keilloltz, J.G. Morgan, W.E. Browning, Effect of Radiation on Corrosion of Structural Materials by Molten Fluorides, Oak Ridge National Laboratory, ORNL-2373, 1957.

[11] J.R. Keiser, Compatibility Studies of Potential Molten-Salt Breeder Reactor Materials in Molten Fluoride Salts, Oak Ridge National Laboratory, ORNL/TM-5783, 1977.

[12] J.R. Keiser, Status of Tellurium-Hastelloy N Studies in Molten-Fluoride Salts, Oak Ridge National Laboratory, ORNL/TM-6002, 1977.

[13] J.R. Keiser, J.H. DeVan, D.L. Manning, The Corrosion of Type 316 Stainless Steel to Li2BeF4, Oak Ridge National Laboratory, ORNL/TM-5782, 1977.

[14] J.W. Koger, Mass Transfer Between Hastelloy N and a Molten NaBF4 Mixture in a Thermal Convection Loop, Oak Ridge National Laboratory, ORNL/TM-4271, 1972. ORNL/TM-4271.

[15] J.W. Koger, A Forced-Circulation Loop for Corrosion Studies: Hastelloy N Compatibility with NaBF4-NaF, Oak Ridge National Laboratory, ORNL/TM-4221, 1972.

[16] J.W. Koger, Alloy Compatibility with LiF-BeF2 Salts Containing ThF4 and UF4, Oak Ridge National Laboratory, ORNL/TM-4286, 1972.

[17] J.W. Koger, Corrosion and Mass Transfer Characteristics of NaBF4-NaF in Hastelloy-N, Oak Ridge National Laboratory, ORNL/TM-3866, 1972.

[18] J.W. Koger, Effect of FeF2 Addition on Mass Transfer in a Hastelloy N - LiF-BeF2-UF4 Thermal Convection Loop System, Oak Ridge National Laboratory, ORNL/TM-4188, 1972.

[19] J.W. Koger, Evaluation of Hastelloy N Alloys After Nine Years Exposure to Both a Molten Fluoride Salt and Air at Temperatures from 700 to 560 C., Oak Ridge National Laboratory, ORNL/TM-4189, 1972.

[20] J.W. Koger, Corrosion of Type 304L Stainless Steel and Hastelloy-N by Mixtures of BF3, Air, and Argon, Oak Ridge National Laboratory, ORNL/TM-4172, 1972.

[21] J.W. Koger, A.P. Litman, Compatability of Hastelloy N and Croloy 9M with NaBF4-NaF-KBF4 (90-4-6 mole %) Fluoroborate Salt, Oak Ridge National Laboratory, ORNL/TM-2490, 1969.

[22] J.W. Koger, A.P. Litman, Mass Transfer Between Hastelloy N and Haynes Alloy No. 25 in a Molten Sodium Fluoroborate Mixture, Oak Ridge National Laboratory, ORNL/TM-3488, 1971.

[23] J.W. Koger, A.P. Litman, Compatibility of Molybdenum-Base Alloy TZM, with LiF-BeF2-ThF4-UF4 (68-20-11.7-0.3) at 1100 C, Oak Ridge National Laboratory, ORNL/TM-2724, 1969.

[24] A.P. Litman, A.E. Goldman, Corrosion Associated with Fluorination in the Oak Ridge National Laboratory Fluoride Volatility Process, Oak Ridge National Laboratory, ORNL-2832, 1961.

[25] A.P. Litman, A.E. Goldman, Corrosion Associated with Hydrofluorination in the Oak Ridge National Laboratory Fluoride Volatility Process, Oak Ridge National Laboratory, ORNL-2833, 1961.

[26] W.D. Manly, G.M. Adamson, J.H. Coobs, J.H. DeVan, D.A. Douglas, E.E. Hoffman, P. Patriarca, Aircraft Reactor Experiment - Metallurgical Aspects, Oak Ridge National Laboratory, ORNL-2349, 1957.

[27] W.R. Martin, H.E. McCoy, J.R. Weir, Production of a Low-Boron Heat of Hastelloy N, Oak Ridge National Laboratory, ORNL/TM-1146, 1965.

[28] W.R. Martin, J.R. Weir, Effect of Elevated Temperature Irradiation on the Strength and Ductility of the Nickel-Base Alloy, Hastelloy-N, Oak Ridge National Laboratory, ORNL/TM-1005, 1965.

[29] A.L. Matthews, C.F.J. Baes, Oxide Chemistry and Thermodynamics of Molten Lithium Fluoride - Beryllium Fluoride by Equilibriation with Gaseous Water - Hydrogen Fluoride Mixtures, Oak Ridge National Laboratory, ORNL/TM-1129, 1965.

[30] H.E. McCoy, Status of Materials Development for Molten-Salt-Reactors, Oak Ridge National Laboratory, ORNL/TM-5920, 1978.

[31] H.E. McCoy, An Evaluation of the MSRE Hastelloy N Surveillance Specimens - Second Group, Oak Ridge National Laboratory, ORNL/TM-2359, 1969.

[32] H.E. McCoy, An Evaluation of the Molten-Salt Reactor Experiment Hastelloy N Surveillance Specimens - Fourth Group, Oak Ridge National Laboratory, ORNL/TM-3063, 1971.

[33] H.E. McCoy, An Evaluation of the MSRE Hastelloy-N Surveillance Specimens - First Group, Oak Ridge National Laboratory, ORNL/TM-1997, 1967.

[34] H.E. McCoy, Infleunce of Titanium, Zirconium, and Hafnium Additions on the Resistance of Modified Hastelloy N to Irridation Damage at High Temperature - Phase I, Oak Ridge National Laboratory, ORNL/TM-3064, 1971.

[35] H.E. McCoy, Studies of the Carbon Distribution in Hastelloy-N, Oak Ridge National Laboratory, ORNL/TM-1353, 1966.

[36] H.E. McCoy, An Evaluation of the Molten-Salt Reactor Experiment Hastelloy-N Surveillance Specimens - Third Group, Oak Ridge National Laboratory, ORNL/TM-2647, 1970.

[37] H.E. McCoy, Effects of Irradiation on the Mechanical Properties of Two Vacuum Melted Heats of Hastelloy N, Oak Ridge National Laboratory, ORNL/TM-2043, 1968.

[38] H.E. McCoy, Influence of Several Metallurgical Variables on the Tensile Properties of Hastelloy N, Oak Ridge National Laboratory, ORNL-3661, 1964.

[39] H.E. McCoy, Influence of Various Gaseous Environments on the Creep-Rupture Properties of Nuclear Materials for High-Temperature Service, Oak Ridge National Laboratory, ORNL/TM-0326, 1962.

[40] H.E. McCoy, D.T. Bourgette, Influence of Aging on the Impact Properties of Hastelloy N, Haynes Alloy no. 25, and Haynes Alloy no. 188, Oak Ridge National Laboratory, ORNL/TM-4380, 1973.

[41] H.E. McCoy, D.A. Canonico, Preirridation and Postirridation Mechanical Properties of Hastelloy N Welds, Oak Ridge National Laboratory, ORNL/TM-2483, 1969.

[42] H.E. McCoy, R.W. Gunkel, G.M. Slaughter, Tensile Properties of Hastelloy-N Welded After Irradiation, Oak Ridge National Laboratory, ORNL/TM-2858, 1970.

[43] H.E. McCoy, B. McNabb, Intergranular Cracking of INOR-8 in the MSRE, Oak Ridge National Laboratory, ORNL-4829, 1972.

[44] H.E. McCoy, B. McNabb, Post-Irradiation Examination of Materials from the MSRE, Oak Ridge National Laboratory, ORNL/TM-4174, 1972.

[45] H.E. McCoy, J.R. Weir, Materials Development for Molten-Salt Breeder Reactors, Oak Ridge National Laboratory, ORNL/TM-1854, 1967.

[46] H.E. McCoy, J.R. Weir, In- and Ex-Reactor Stress-Rupture Properties of Hastelloy N Tubing, Oak Ridge National Laboratory, ORNL/TM-1906, 1967.

[47] H.E. McCoy, J.R. Weir, R.L. Beatty, W.H. Cook, C.R. Kennedy, A.P. Litman, R.E. Gehlbach, C.E. Sessions, J.W. Koger, Materials for Molten-Salt Reactors, Oak Ridge National Laboratory, ORNL/TM-2511, 1969.

[48] L.S. Richardson, D.C. Vreeland, W.D. Manly, Corrosion by Molten Fluorides, Oak Ridge National Laboratory, ORNL-1491, 1953.

[49] R.C. Schulze, W.H. Cook, R.B.I. Evans, J.L. Crowley, INOR-8-Graphite-Fused Salt Compatibility Test, Oak Ridge National Laboratory, ORNL-3124, 1961.

[50] C.E. Sessions, E.E. Stansbury, Thermal Stability of Titanium-Modified Hastelloy N at 650 and 760 C, Oak Ridge National Laboratory, ORNL/TM-3321, 1971.

[51] G.M. Slaughter, P. Patriarca, R.E. Clausing, Welding of Nickel-Molybdenum Alloys, Oak Ridge National Laboratory, ORNL-2760, 1959.

[52] R.W. Swindeman, Mechanical Properties of INOR-8, Oak Ridge National Laboratory, ORNL-2780, 1961.

[53] R.E. Thoma, Chemical Aspects of MSRE Operations, Oak Ridge National Laboratory, ORNL-4658, 1971.

[54] L.M. Toth, Containers for Molten Fluoride Spectroscopy, Oak Ridge National Laboratory, ORNL/TM-2047, 1967.

[55] W.C. Tunnell, Compatibility Tests of Materials for Use in Bearings, Seals, and Valves in Fused Fluoride Salts at 1200F, Oak Ridge National Laboratory, ORNL-2103, 1956.

[56] J.T. Vernard, Tensile and Creep Properties of INOR-8 for the Molten-Salt Reactor Experiment, Oak Ridge National Laboratory, ORNL/TM-1017, 1965.

[57] J.R. Weir Jr., D.A. Douglas, W.D. Manly, Inconel as a Structural Material for a High-Temperature Fused-Salt Reactor, Oak Ridge National Laboratory, ORNL-2264, 1957.

[58] J.R. Weir, J.O. Stiegler, E.E. Bloom, Irradiation Behavior of Cladding and Structural Materials, Oak Ridge National Laboratory, ORNL/TM-2258, 1968.